

Prospects for Systematic Planetary Nebulae Detection with the Census of the Local Universe Narrowband Survey

RONG DU ,^{1,2,3} DAVID O. COOK ,² SOUMYADEEP BHATTACHARJEE ,¹ SHRINIVAS R. KULKARNI ,^{1,4}
 CHRISTOFFER FREMLING ,¹ DAVID L. KAPLAN ,⁵ MANSI M. KASLIWAL ,¹ RUSS R. LAHER ,² FRANK J. MASCI ,²
 DAVID L. SHUPE ,² AND CHAORAN ZHANG ,⁶

¹Cahill Center for Astronomy and Astrophysics, California Institute of Technology, Pasadena, CA 91125, USA

²IPAC, California Institute of Technology, 1200 E. California Boulevard, Pasadena, CA 91125, USA

³Kavli Institute for Astronomy and Astrophysics, Peking University, Beijing 100871, China

⁴Department of Astronomy, Cornell University, Ithaca, NY 14853, USA

⁵Department of Physics, University of Wisconsin-Milwaukee, PO Box 413, Milwaukee, WI 53201, USA

⁶Center for Gravitation, Cosmology, and Astrophysics, Department of Physics, University of Wisconsin-Milwaukee, PO Box 413, Milwaukee, WI 53201, USA

ABSTRACT

We investigate the efficacy of a systematic planetary nebula (PN) search in the Census of the Local Universe (CLU) narrowband ($\text{H}\alpha$) survey that covers a considerably larger sky region of above declination -20° than most previous surveys. Using PNe observed by the Isaac Newton Telescope Photometric $\text{H}\alpha$ Survey (IPHAS) as validation, we are able to visually recover 432 out of 441 cataloged PNe (98%) within the CLU dataset, with 5 sources having unusable CLU images and 4 missed due to limitations of imaging quality. Moreover, the reference PNe are conventionally divided into three PN classes in decreasing order of identification confidence given their spectra and morphologies. We record consistently high recovery rate across all classes: 95% of True, 71% of Likely, and 81% of Possible sources are readily recovered. To further demonstrate the ability of CLU to find new PNe, we undertake a preliminary search of compact PNe within a sub-region of the validation catalog, mainly utilizing the significance of narrow-band colors (Σ) as a metric for identification. In a 200 deg^2 region, we search the CLU source catalog and find 31 PN candidates after automated and visual scrutiny, of which 12 are new sources not appearing in previous studies. As a demonstration of our ongoing follow-up campaign, we present medium-resolution optical spectra of six candidates and notice that four of them show emission signatures characteristic of confirmed PNe. As we refine our selection methods, CLU promises to provide a systematic catalog of PNe spanning 2/3 of the sky.

Keywords: Planetary nebulae (1249), H II regions (694), Surveys (1671), H alpha photometry (691)

1. INTRODUCTION

Planetary nebulae (PNe) represent the late phase in the life cycle of low- to intermediate-mass stars (1 to 8 M_\odot ; e.g., Kwok 2005). They offer valuable insights into the short phase of stellar evolution, and the composition and related dynamics of the interstellar medium. The

relatively brief evolutionary stage, spanning approximately 25,000 years (e.g., Jacob et al. 2013; Badenes et al. 2015; Le Dû et al. 2022), encapsulates the transition from the asymptotic giant branch to white dwarfs (Paczyński 1971a,b). The hot white dwarf ionizes the surroundings and aids in the expansion of the ejected stellar shell through its winds (e.g., Kwok et al. 1978; Frank et al. 1990). The ionized shell then forms a PN with robust nebular emission lines, whereas the white dwarf forms the central star of the PN (CSPN) with a temperature exceeding $\sim 10^4$ to even 10^5 K (e.g., Frew & Parker 2010). The visibility of these emission lines over

Corresponding author: Rong Du
 durong@alumni.pku.edu.cn
 dcook@ipac.caltech.edu

considerable distances allows for the determination of PNe sizes and expansion velocities, thereby facilitating more precise exploration of the time-scales associated with the ejection (e.g., Iben 1995). The elemental composition of the ejecta provide direct insights into stellar evolution and chemical enrichment in galaxies (e.g., Dopita et al. 1997; Maciel & Costa 2003). On a cosmic scale, the bright-end exponential cut-off of the luminosity function of PNe serves as a standard candle for calibrating cosmological distances (e.g., Ford & Jenner 1978; Ciardullo et al. 1989; Jacoby 1989, 1997; Ciardullo et al. 2002; Scheuermann et al. 2022).

The discovery of the first known PN in 1764 (“Dumbbell” Nebula, Messier 27) by Charles Messier marked the beginning of a quest to understand these enigmatic objects. Subsequent decades saw the compilation of the first catalogs of PNe by Abell (1966) and also Perek & Kohoutek (1967) whose sources were robustly confirmed with spectroscopic studies. Recent discoveries, primarily propelled by extensive optical surveys focusing on the H α emission line, have substantially augmented the list of candidates as well as confirmed PNe. Examples include the Macquarie-AAO-Strasbourg H α (MASH) Survey Catalog (Parker et al. 2006a; Miszalski et al. 2008) derived from the AAO/UKST SuperCOSMOS H α survey (SHS; Parker et al. 2005), and the Isaac Newton Telescope (INT) Photometric H α Survey (IPHAS; Drew et al. 2005). Further contributions to the PN population come from surveys in the Galactic bulge region, such as those conducted by Boumis et al. (2006), Górný (2006), the Deep Sky Hunters consortium (e.g., Jacoby et al. 2010; Kronberger et al. 2012, 2014, 2016), and the amateur community (e.g., Acker et al. 2012). These diverse discoveries have been collated into the Hong Kong/AAO/Strasbourg/H α (HASH) PN database (Parker et al. 2014, 2016; Bojićić et al. 2017).

Despite recent advancements that have amply increased the known Galactic PN population, a significant gap of potentially up to an order of magnitude remains when comparing the number of known PNe (~ 3900) to the theoretically predicted number ($\sim 6,600$ to $60,000$; e.g., Frew & Parker 2005; Moe & De Marco 2006; Jacoby et al. 2010; Frew 2017). This discrepancy may introduce bias in analysis and hinders attempts to characterize the global PN population accurately. Therefore, the discovery of new PNe is necessary to enhance the census of this essential celestial object and its luminosity function.

To efficiently expand the catalog of known PNe (e.g., see Kwitter & Henry 2022; Parker 2022), we leverage imaging data from the Census of the Local Universe (CLU; Cook et al. 2019) narrowband survey which was conducted as part of the intermediate Palomar Tran-

sient Factory (iPTF; Law et al. 2009; Rau et al. 2009) program. While the primary science case of CLU endeavors to survey the local Universe for galaxies with distances out to 200 Mpc ($z \sim 0.05$) across 2/3 of the sky (26,470 deg 2 ; see Cook et al. 2019 for details), the survey holds the potential in unveiling all types of galactic H α emission-line objects including PNe. With its large sky coverage, the survey is ideal for exploring sky regions that lie outside the footprint of previous surveys like SHS (Parker et al. 2005) and IPHAS (Drew et al. 2005) to contribute a homogeneous PNe sample spanning 2/3 of the entire sky.

As a pilot study, we investigate the prospects of discovering new PNe with CLU in this paper. The rest of the paper is organized as follows. We introduce the CLU survey in Section 2. In Section 3, we test the efficacy of detecting PNe in CLU-H α images by constructing a validation catalog using PNe detectable in IPHAS and quantifying its recovery rate. To further demonstrate the ability of the CLU database, we conduct a preliminary search within the sky field of the validation catalog to find more PNe as described in Section 4. We discuss the caveats of our PNe search and the future prospective of CLU in Section 5. Finally, we present our conclusions in Section 6.

2. THE CLU H α SURVEY

As detailed in Cook et al. (2019), the CLU survey represents a comprehensive endeavor to catalog and characterize H α emitting galaxies across the sky above -20° declination. The survey is conducted on the 1.2 m Oschin Telescope at Palomar Observatory, employing four adjacent narrowband H α filters (hereafter, H α 1–H α 4) with their central wavelengths at 6563.7 Å, 6642.7 Å, 6717.6 Å, and 6808.6 Å, respectively. The CLU survey is capable of detecting H α emission lines down to 1.6×10^{-14} erg s $^{-1}$ cm $^{-2}$ (143.95 R with 2.5'' photometric aperture radius) at 90% completeness (Cook et al. 2019, 2024; submitted). It has been successfully used for finding galaxies and has discovered several interesting objects like blue compact dwarfs, green peas (e.g., Lintott et al. 2008), and Seyfert galaxies (Cook et al. 2019).

The scope of the survey, however, need not be limited to its goal on galaxies. In fact, the survey design is apt to search for many galactic H α emission-line objects, with our work here focusing on PNe. Interestingly, alongside galaxies, a known PN (H 4-1; Haro 1951) has also been recovered in one of the CLU preliminary fields (Cook et al. 2017, 2019). The magnitude, m , of the object in the rest-frame H α filter (“H α 1” or “On” filter) compared to the adjacent filter (“H α 2” or

“Off” filter) is $m_{\text{H}\alpha 1} - m_{\text{H}\alpha 2} = -3.05$, which implies a very significant detection of this object in the CLU survey (Cook et al. 2019). We note that this PN is situated at a high Galactic latitude of $b = 88.14757^\circ$ and $l = 49.3065^\circ$, which is outside the footprint of the previous major surveys, thus supporting the effectiveness of CLU in exploring these areas in the sky. Its measured H α -line flux and equivalent width from the CLU data are 1.21×10^{-12} ergs $^{-1}$ cm $^{-2}$ and 1200 Å, respectively.

Table 1. Comparison between CLU and IPHAS

Property	CLU	IPHAS
Location	San Diego, USA	La Palma, Spain
Observatory	Palomar	Roque de los Muchachos
Telescope	Samuel Oschin	INT
Aperture	1.2 m	2.5 m
Instrument	PTF Survey Camera	Wide Field Camera
Pixel Scale	1.01'' pixel $^{-1}$	0.33'' pixel $^{-1}$
Filters	H α 1, H α 2, H α 3, H α 4 6563.7 6642.7 6717.6 6808.6 84.6 85.5 95.1 98.7	r', i', H α 6568
H α λ (Å)		
H α $\Delta\lambda$ (Å)	60 s	120 s
Exposure Time	AB	Vega
Magnitudes	19.1 ± 0.5	20.3 ± 0.3
Detection Limit	29° < l < 215°	
Longitude Range	Decl. > -20°	-5° < b < +5°
Latitude Range	2009 – 2017/03	2003/08 – 2012/11
Observing Period		

NOTE— Col. (1): Properties of interest. “H α λ ” denotes the central wavelength of the H α filters, “H α $\Delta\lambda$ ” indicates the full width at half-maximum, and “Detection Limit” presents the mean and standard deviations of 5 σ detection limits in magnitudes. Col. (2): Relevant values for the CLU survey retrieved from Law et al. (2009); Rau et al. (2009); Cook et al. (2019) and Cook et al. (submitted). Data for the four H α filters are listed respectively from top to bottom in relevant sections for “H α λ ”, “H α $\Delta\lambda$ ”, and “Detection Limit”. Additionally, although observations using the H α 3 and H α 4 filters cover the sky above -20° declination, the Galactic plane ($|b| \lesssim 3^\circ$) is avoided (see Cook et al. 2019, Figures 2 and 3). Col. (3): Relevant values for IPHAS retrieved from Drew et al. (2005); González-Solares et al. (2008); Barentsen et al. (2014).

3. RECOVERING PLANETARY NEBULAE

We proceed to validate the technical feasibility and quantify the effectiveness of systematic PNe detection within CLU-H α images via visual inspections of a catalog of PN candidates observed in the IPHAS survey. The three primary reasons for referring to this catalog are: (1) it stands as the largest H α survey in the northern Galactic plane; (2) it has undergone systematic study for PNe detection, contributing both methodologically and in terms of source inclusion to the HASH database; and, (3) it provides deeper data compared to the CLU survey, ensuring sufficiently reliable validations for our visual recovery. As detailed in the following sections, we scrutinize corresponding CLU-H α images to determine if the object has been satisfactorily detected by CLU, and then conduct a statistical analysis.

3.1. The INT Photometric H α Survey

The IPHAS is a comprehensive photometric survey of the northern Galactic plane covering Galactic latitudes of $|b| < 5^\circ$ and longitudes of $29^\circ < l < 215^\circ$ (for details, see Drew et al. 2005; Barentsen et al. 2014). Utilizing the 2.5 m INT at La Palma in the Canary Islands of Spain with a Field of View (FoV) of $34' \times 34'$, the survey employs photometric filters including the Sloan r (centered at 6240 Å, 30 s exposure), the Sloan i (7743 Å, 10 s), and the H α (6568 Å, 120 s) (Drew et al. 2005). The coverage of H α point sources is down to a magnitude of 20.3 at the 5- σ level (Vega system; see Barentsen et al. 2014) against 19.1 with CLU-H α 1 stacked images (Cook et al. 2019; 2024, submitted). The depth of IPHAS is further coupled with the sensitivity for extended emission down to an H α surface brightness limit of 2.5×10^{-16} erg cm $^{-2}$ s $^{-1}$ arcsec $^{-2}$ (against 1.6×10^{-14} erg s $^{-1}$ cm $^{-2}$ with CLU). Such high sensitivity of IPHAS facilitates its detection of emitting nebulae and their morphological structures in the more obscured and crowded regions of the Galactic plane.

In Table 1, a detailed comparison between IPHAS and CLU is presented. Evidently, the IPHAS is a deeper survey than CLU. However, the advantage of the latter is its much wider sky coverage, enabling exploration of the yet unexplored parts of the sky.

3.2. The Validation Catalog

IPHAS provides imaging data for a plethora of H α emitting sources within which various studies have reported their discovering of PN candidates or even confirmed PNe with spectroscopic analysis (e.g., Corradi et al. 2005; Viironen et al. 2009a,b; Sabin et al. 2010, 2014). To construct the validation catalog, we retrieved a total of 441 labeled Galactic PNe detectable in IPHAS

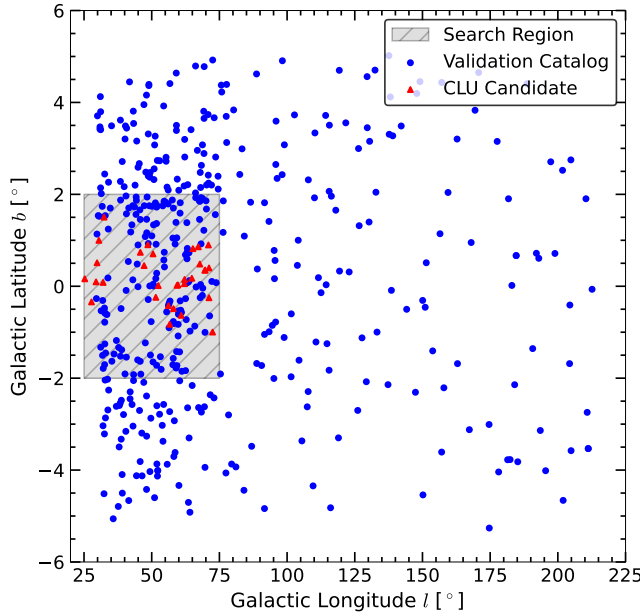


Figure 1. The sky locations in Galactic coordinates. The blue dots represent the planetary nebula candidates in the validation catalog. The red dots represent candidates from our preliminary search on CLU which is explained in Section 4. The shaded region depicts the sky region of the preliminary search.

from the HASH database¹ (data retrieved in October 2023; Parker et al. 2016).

Three searches contribute significantly to the catalog. The validation catalog encompasses 132 PNe originally observed by Acker et al. (1992) but subsequently detected in IPHAS in succeeding works. As part of a systematic effort leveraging the IPHAS data, Viironen et al. (2009a) and Viironen et al. (2009b) discovered 70 sources using a semi-automated methodology that involved data cleaning primarily with cuts on IPHAS colors and also source selection based on both IPHAS and Two Micron All Sky Survey (2MASS, Skrutskie et al. 2006) color indices. After color selection, all remaining objects were visually classified in their IPHAS images. A more recent work by Sabin et al. (2014) contributed 105 additional extended sources through visual inspection of IPHAS $\text{H}\alpha - r$ difference map mosaics on two scales of binned data: initially by 5×5 pixels ($\sim 1.7'' \text{ pixel}^{-1}$), and then by 15×15 pixels ($\sim 5'' \text{ pixel}^{-1}$). This coarser binning aided in resolving low-surface-brightness objects effectively, reaching the detection limit of IPHAS as outlined by Sabin et al. (2010). For information on other references of the validation catalog, see Column (13) of Table A1 in Appendix A.

¹ <http://202.189.117.101:8999/gpne/>

In the HASH database, sources are documented with their name, coordinates in both Equatorial and Galactic systems, diameters of major (D_{maj}) and minor (D_{min}) axes, main and subsidiary morphology, position angle, multi-band fluxes, PN class, and reference catalog or article. The spatial distribution of all sources in the validation catalog is visualized in Galactic coordinates in Figure 1.

In HASH terminology, morphologies and classes adhere to a convention initiated by MASH (Parker et al. 2006b). Primary morphological classifications “E; R; B; I; A; S” denote Elliptical, Round, Bipolar, Irregular, Asymmetric, and quasi-Stellar (unresolved or barely resolved) PNe, respectively. Sub-morphology classifiers “a; m; p; r; s” are employed for “a”symmetries, “m”ultiple shells or external structures, “p”oint symmetry, well-defined “r”ing structures or annuli, and resolved, internal “s”tructure, respectively. The PN class in terms of “T/L/P” denote the quality of sources during the identification process (e.g., Parker et al. 2005; Parker 2022):

True “T”: spectroscopically and morphologically well-defined PNe across multi-wavelengths, and sometimes with an obvious blue CSPN;

Likely “L”: not completely conclusive identification spectroscopically or morphologically;

Possible “P”: non-conclusive identification. The quality of spectroscopic or morphological data can resolve the source but cannot rule out contaminants like H II regions, etc.

Out of the 441 sources in the validation catalog, 317 are classified as T, 49 as L, and 75 as P PNe, respectively.

3.3. Visual Inspection

We conduct systematic visual inspections of images from CLU- $\text{H}\alpha$ centered on objects in the validation catalog. We note here that our goal is to determine the feasibility of finding PNe in the CLU survey, and that additional discovery methodologies for new PNe will be explored later in this paper (see Section 4) and in future efforts. Since no spectroscopic follow-up is conducted, we refrain from adopting the “T-L-P” system used by HASH to register PNe status. Instead, we assign each source a classification grade based on both the quality of our visual detection of nebular emission and the confirmation of its morphology documented in previous catalogs:

- (A) Obvious nebular signal showing clear morphology, matching the known information.

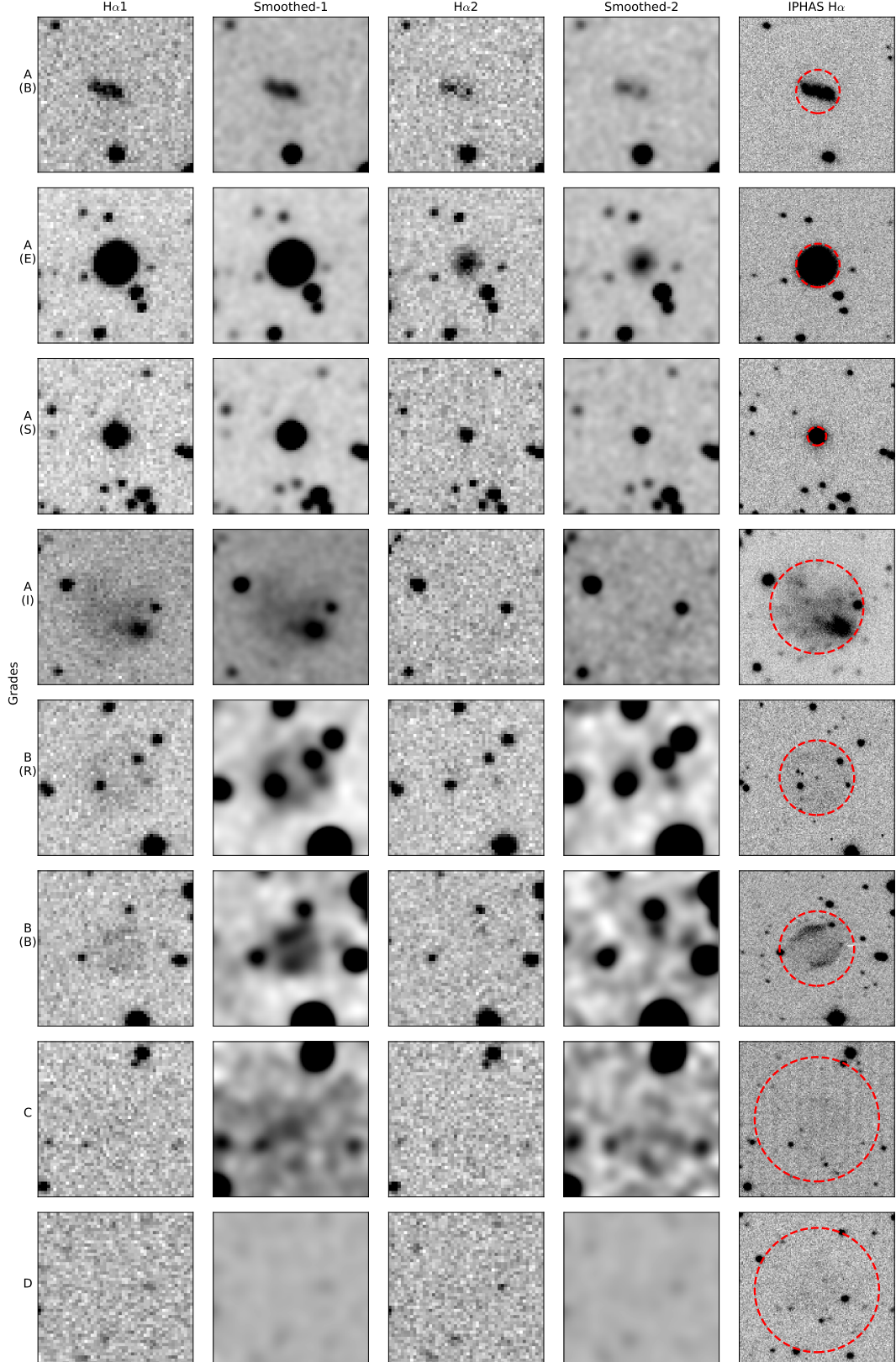


Figure 2. Example images of H α emission-line sources from the four PN classification grades from A to D (in the decreasing order of the confidence, c.f. Section 3.3). The five columns show images from the first H α band, smoothed H α 1, the second H α band, smoothed H α 2, and the respective IPHAS H α images. The red circles indicate the nebular regions. For visualization, the smoothing value is one pixel for grade A sources, and two pixels for grades B, C, and D sources. All images have a FoV of 50''. **Row 1:** Images of a bipolar grade A source (Te10, HASH ID 4372). **Row 2:** An elliptical A source (K 3-90, 653). **Row 3:** A quasi-stellar A source (K 3-69, 705). **Row 4:** An irregular A source (IPHASX J193740.4+203547, 10061). **Row 5:** A round B source (IPHASX J013108.9+612258, 8450). **Row 6:** A bipolar B source (IPHASX J194301.3+215424, 8566). **Row 7:** A grade C source (IPHASX J184030.1–003822, 8478) which is difficult to identify without referring to the IPHAS images showing the location of the emissions. **Row 8:** An undetected grade D source (IPHASX J185225.0+080843, 15651).

- (B) Clear detection of some part of the nebular emission with confident verification of the morphology. Additional visualizations (e.g., Gaussian smoothing, rebinning) and careful inspection are needed.
- (C) Possible detection of only part of the nebular emission where the morphology cannot be robustly verified even when referring to the validation catalog.
- (D) No detection of the nebula or any associated morphology.

The grading system is based on the primary emission of PNe in H α (CLU-H α 1). For grade A sources, the recovery is straightforward. For grade B and C sources, we provide the reasons for such grading for each source. For grade D sources, where the source is undetected regardless of fine-tuning the image visualization, we explain the reason of detection failures for each specific source. Sources with grade A or B are considered readily recovered. Grade C sources are only marginally recovered.

Our procedure starts by examining CLU-H α imaging at the coordinates of each validation object, where we adjust the FOV to approximately 1.5-2 times the major diameter of the nebula. If we can directly observe the source or, after contrast adjustments, discern a nebulosity and its documented morphology, the source is classified as grade A. If confirmation is challenging, we apply Gaussian smoothing and designate the source as grade B if the whole nebulosity or part of its morphology becomes visible. For sources that remain undetected, we refer to spectra, notes, and multi-band images in the HASH database, and adjust the image visualization parameters (image center, viewing contrast, σ of Gaussian smoother, etc.) accordingly. Detected sources are in grade C, while those undetected remain in grade D. Examples are shown for the four respective grades in Figure 2.

Including five sources with unusable, masked CLU images that have flat photon distribution, we present the full result of the recovery in Table A1 (Appendix A). Overall, out of 441 validation sources, we have recovered 335 A (76%), 62 B (14%), and 35 C (8%) sources, and labelled 4 D sources (0.9%). Thus, the majority of sources (90%) fall in grades A and B as readily recovered cases. Including grade C, we have in total 98% validation sources successfully recovered, which demonstrates the ability of CLU-H α to reproduce previous discoveries, implying its viability for further research. A histogram of classification grades is shown in Figure 3. In PN classes, 95% of True, 71% of Likely, and 81% of Possible sources are readily recovered, implying the consistency of high recovery rate across all classes. The fact that 85% “T” sources are labelled as grades A and

B suggests that most of the bona fide PNe are easily recovered by CLU. For the four grade D sources:

IPHASX J061602.5+175920 (class “P”): It is a very large nebula ($D_{\text{maj}} = 274''$) of very low surface brightness. CLU documented three single epoch images in the relevant sky region, from which a stacked image was created, but no nebular emission is detected. Two of the CLU exposures have masked regions or bad pixels in the nebular region, diminishing the quality of the “stacked image” to the same as the third single epoch unmasked image. Additionally, several bright point sources in the FoV of the unmasked epoch further restrain our visualization techniques to improve the contrast to reveal the emission region. Nevertheless, the source itself requires further observations for its nature to be determined.

IPHASX J185225.0+080843 (class “T”, reported by Sabin et al. 2014): The source is very faint with low signal-to-noise ratio (S/N) in the IPHAS image. The relevant sky region was only observed once in the CLU-H α imaging data. This source is selected as an example to demonstrate our classification grades in Figure 2.

Pa J1906.9+0413 (class “L”): It was originally discovered by the Deep Sky Hunters community (Kronberger et al. 2006; Jacoby et al. 2010). Similar to the previous source, it has very weak IPHAS detection and only one CLU exposure. Nevertheless, it is well-resolved in the Wide-field Infrared Survey Explorer (WISE; Wright et al. 2010) bands, implying possible obscuration along the line of sight.

IPHASX J194745.5+270150 (class “P”): It is a large ($D_{\text{maj}} = 207''$), very faint, elliptical nebula observed four times by CLU. However, three of the four exposures are masked. The source also has an extremely flat spectral continuum around H α , which make it hard to determine whether a real emitter with little H α excess or the background with no detection occupies the image.

3.4. Statistics on the Recovery

We compute Spearman’s rank correlation coefficient between the classification grades used in our study and the HASH PN classes, yielding $\rho = 0.3297$. A subsequent *T*-test returns a p-value of $p < 0.001$, which indicates a weak correlation between grades and classes. Better PN class means more prominent source and

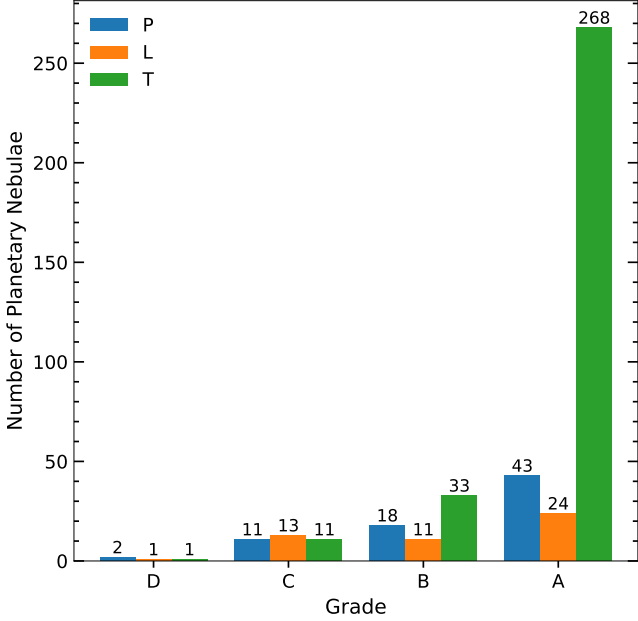


Figure 3. Histogram of planetary nebula candidates in the validation catalog with respect to different grades (A, B, C, and D). Within each grade, sources are divided according to their classes of True, Likely, and Possible.

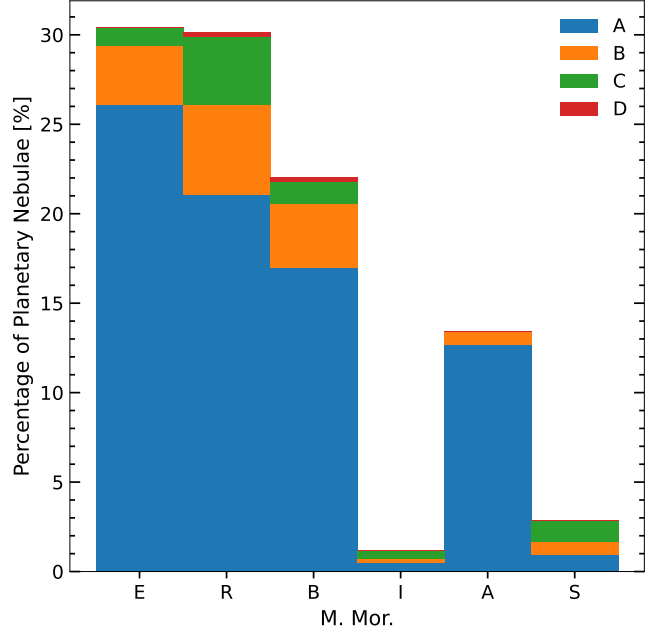


Figure 5. Histogram of planetary nebula candidates in the validation catalog with respect to different main morphology (M. Mor.), where E, R, B, I, A, and S stands for the M. Mor. of Elliptical, Round, Bipolar, Irregular, Asymmetric, and quasi-Stellar (unresolved or barely resolved), respectively. Sources are divided according to their grades of A, B, C, and D.

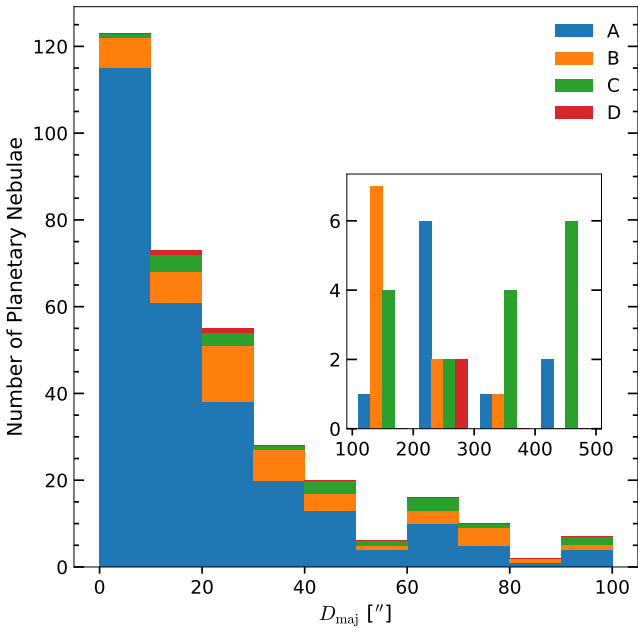


Figure 4. Histogram of planetary nebula candidates in the validation catalog with respect to different major diameters (D_{maj}). Sources are labeled according to their grades of A, B, C, and D. In the figure, smaller nebulae are usually labeled with a higher grade ranking.

clearer morphology, which increases the chance of our visual detection, hence a higher grade.

Additionally, the apparent major diameter (D_{maj}) of the nebula may influence detection. Excluding sources without reported diameters in the validation catalog, we present a histogram of D_{maj} in Figure 4. With a Spearman's correlation coefficient $\rho = -0.4277$ between grades and D_{maj} and $p < 0.001$ in a subsequent T -test, we observe a weak-to-moderate negative correlation between grades and D_{maj} of the nebulae. A possible explanation would be that lots of larger nebulae may have lower surface brightness making them more difficult to detect.

The intricate and diverse morphology of PNe also serves as a vital classifier. Studies have suggested that the morphology of PNe can be indicative of the properties of their progenitor stars, mass ejection mechanisms, and multiple shaping processes involving external torques from close or merging binary companions, or the emergence of magnetic fields embedded in dense outflowing stellar winds (e.g., Balick & Frank 2002; Parker et al. 2006a; Miszalski et al. 2009). We present a histogram of main morphology categories (M. Mor.) in Figure 5, and notice the absolute dominance of those PNe with more symmetrical or barely resolvable quasi-stellar shapes. However, we are not able to make a conclusive claim, because a homogeneous sample of Galac-

tic PNe would be needed. Given that IPHAS and SHS are deeper than CLU, our classification grades might be more affected by the resolvability of CLU images than the morphology of the sources.

4. PRELIMINARY SEARCH ON THE CLU SURVEY

Previous analyses have shown that known PNe can be detected from CLU images effectively, whereas in this section, we briefly explore the potential of discovering new PNe in the CLU database. We start with a catalog search for strong emission-line sources in the CLU dataset with $|b| < \pm 2^\circ$ and $l = 25^\circ$ to 75° to identify PN candidates. Subsequent spectroscopic follow-up for six candidates are presented. We recognize that our preliminary search does not aim to offer a systematic and complete CLU PNe list for the selected region, because such discoveries of new PNe based on their nebular emission usually necessitates the combination of several different techniques due to the complex characteristics of PNe including apparent size, morphology, integrated flux, excitation state, CSPN magnitude, and evolutionary state, unless the search focuses on identifying clear nebular regions around known CSPNe (e.g., see the HASH approach in Parker 2022, Section 12.1). However, the exercise we present in this section is sufficient to demonstrate the significant promise of discovering new PNe in CLU.

4.1. The Catalog Search

We utilize the CLU forced photometry source catalog called CLU-FPstack described in Zhang et al. (2024; submitted), where H α fluxes are extracted from the coordinates of Pan-STARRS Data Release 1 (PS1, Chambers et al. 2016) objects regardless of the detection significance in the CLU images. We search CLU-FPstack for PNe, where parameter cut-offs are applied to produce robust candidates. The source catalog search selects candidates primarily based on the “color sigma” (Σ ; Cook et al. 2019), which quantifies the significance that the narrow-band color excess is in one filter above the combined noise of this filter and its adjacent filter. We also ensure the candidates have robust photometry and subsequently robust Σ measurements by applying more cuts on parameters as outlined in the following section. After the selection, we remove contaminants based on their color features and morphology to finally present a list of 31 CLU candidates from the preliminary search.

4.1.1. Source Selection

Widely used for identifying H α emission-line sources (e.g., Bunker et al. 1995; Pascual et al. 2001; Fujita et al. 2003; Sobral et al. 2009, 2012; Ly et al. 2011; Lee et al.

2012; Stroe & Sobral 2015; Cook et al. 2019), Σ is based on the “On-Off” color excess. Our search for PN candidates focuses on the excess of H α emission to the continuum, with H α 1 serving as the “On” band and H α 2 as the “Off” band, which gives:

$$\Sigma = \frac{c_{H\alpha 1} - c_{H\alpha 2}}{\delta}, \quad (1)$$

where $c_{H\alpha 1,2}$ are the counts for H α 1 and H α 2 bands respectively, and δ is the combined sky fluctuations of both filters, of which detailed explanations are provided in Section 3.2 of Cook et al. (2019). Using a fixed photometric aperture with 5'' of diameter, we require $\Sigma > 5.0$ to indicate a positive detection (Cook et al. 2019, 2024; submitted).

Since the source catalog fluxes from forced photometry are based on the locations of the PS1 objects, the offset distance from the PS1 source to the actual CLU source adversely affects the robustness of photometric property calculations. By imposing an upper limit on the distance to the source detected in the stacked image ($dist2stack < 1.5''$), we filter sources whose optical emission centers viewed in PS1 are farther from their positions of H α emission in CLU stacked images. Additionally, we set a minimum H α “On” band magnitude of 11 ($m_{H\alpha} > 11$) to remove saturated sources with poor flux measurements. We further adopt an upper limit for the error of the “On” magnitude to 0.2 ($e_{m_{H\alpha}} < 0.2$) for 5 σ detections.

Prior to applying the cuts to real data, it is useful to estimate its success rate, for which we refer to the previously defined PNe validation catalog (c.f. Section 3.2). Since the region for our preliminary search is within the coverage of the validation catalog as depicted in Figure 1, we can test the cuts on the validation catalog and safely use the results for inferences in our preliminary search region. We apply the cuts to the validation catalog, and notice that 67.9% of sources satisfy $\Sigma > 5.0$, 93.4% have $m_{H\alpha} > 11$, and 96.6% get $e_{m_{H\alpha}} < 0.2$. We present a histogram in Figure 6 to illustrate the cut on the distribution of parameters. We notice that ~ 135 sources with $\Sigma < 5$ are cut off in the left panel, which take up to $\sim 30\%$ of the validation catalog. For cuts on $m_{H\alpha}$ and $e_{m_{H\alpha}}$, a small portion is also discarded. In total, 66.1% sources satisfy all the criteria. Therefore, by applying our cuts, we could potentially cut off $\sim 1/3$ actual PNe through the source catalog search.

In general, we rule out sources with bad photometry or marginal significance by the cuts, but also suffer from missing PNe with less excess in H α or with subtle signals. Implementing the search criteria to CLU-FPstack within $|b| < 2^\circ$ and $25^\circ < l < 75^\circ$, we are able to select $\sim 10,000$ emission-line candidates.

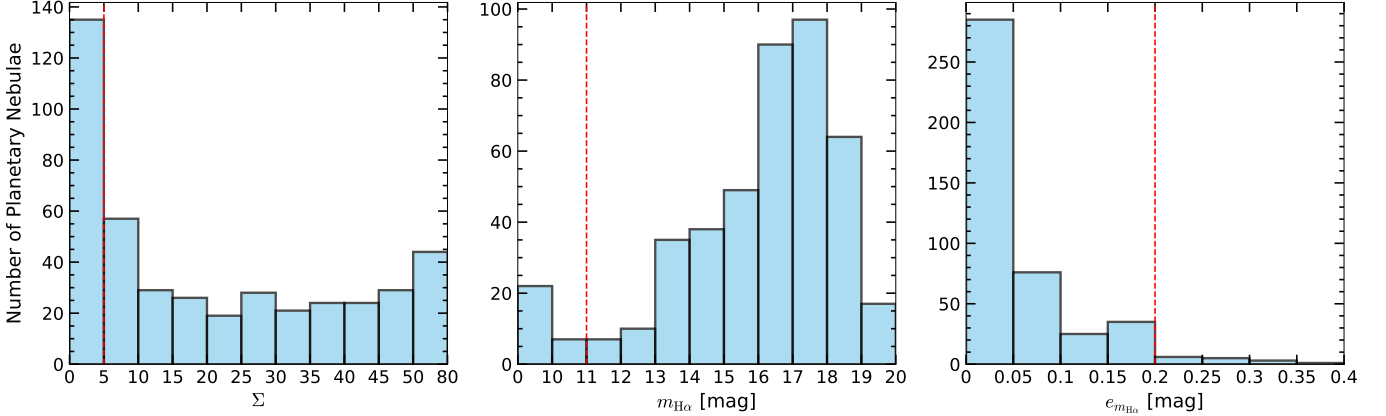


Figure 6. Histogram of planetary nebula candidates in the validation catalog with respect to different color sigma Σ , H α “On” band magnitude $m_{\text{H}\alpha}$, and the error of the “On” magnitude ($e_{m_{\text{H}\alpha}}$). The red dashed line depicts the filtering criteria in the catalog search.

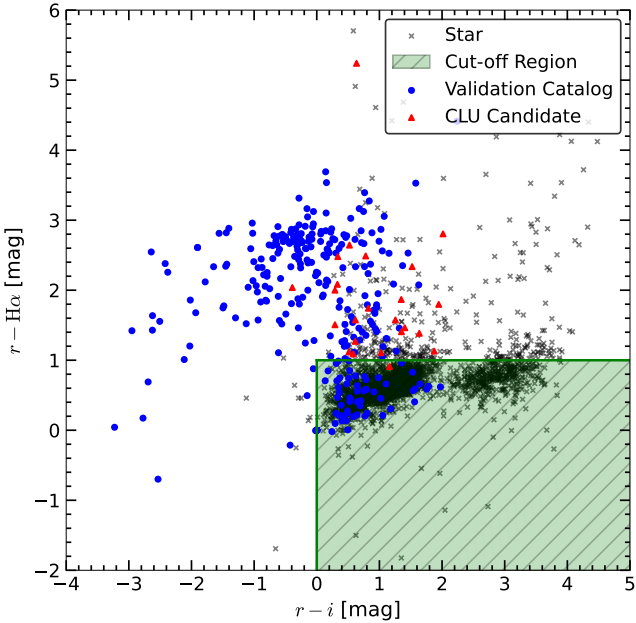


Figure 7. Color-color diagram depicting the $(r - \text{H}\alpha)$ versus $(r - i)$ scatter plot of labelled stars from contaminant removal, planetary nebula candidates in the validation catalog, and candidates from our preliminary search on CLU. The green shaded region represents the region to be cut off through a rough preliminary color cut. All colors in the figure are Kron (1980) magnitudes.

4.1.2. Contaminant Removal

Our straightforward selection criteria add all the H α emission-line sources into the candidate list which may suffer from contamination by various interlopers, such as stars with strong emission lines, H II regions, Wolf-Rayet shells, supernova remnants (SNRs), nearby emission-line galaxies, and artifacts in the CLU images including cosmic rays, hot pixels, satellite streaks, and image ghosts that are not removed during the stacking process. Gen-

eral removal methodology is complicated, involving information from spectroscopy (c.f. Section 5.1). For the preliminary search, we rely on simple color cuts and a few visual inspections to conduct the removal.

Star removal always remains challenging due to its resemblance to compact PNe in their point-like appearances and photometric properties investigated during our detection. Here, we refer to a traditional method of color cuts on two indices (e.g., Viironen et al. 2009a,b). We conduct the H α -PS1 cut-off criterion by removing sources with both $r - i > 0$ and $r - \text{H}\alpha < 1$ as demonstrated in the color-color diagram of $(r - \text{H}\alpha)$ versus $(r - i)$ in Figure 7. The 3400 example stars in the plot are manually classified by us with visual scrutiny on the preliminary search region for testing purposes. Stars in the plot exhibit two distinct clustering trends, indicating the presence of two stellar populations in the CLU survey. For the effectiveness of the cuts, we use the validation catalog constructed in the recovery (Section 3.2) again to calculate that this criterion retains 96% of their documented PN while eliminating 88% of example stars. Applying the color-color cut-off to all 10^4 emission-line candidates, we are able to remove 48% of them as stars.

For the rest of the candidates, we visually label them purely based on the clearness of their nebular morphology and remove the other contaminants mainly consist of artifacts that have singular morphology only existing in one band (48%). During the visual scrutiny, we also refer to images and previous classifications, if any, documented by PS1, Sloan Digital Sky Survey III (SDSS-III; Eisenstein et al. 2011), Set of Identifications, Measurements and Bibliography for Astronomical Data (SIMBAD; Wenger et al. 2000), and HASH, when necessary. With these additional information, if certain sources are firmly considered as a type of contaminant, they are removed by us as well. In the end, ~ 400 sources are iden-

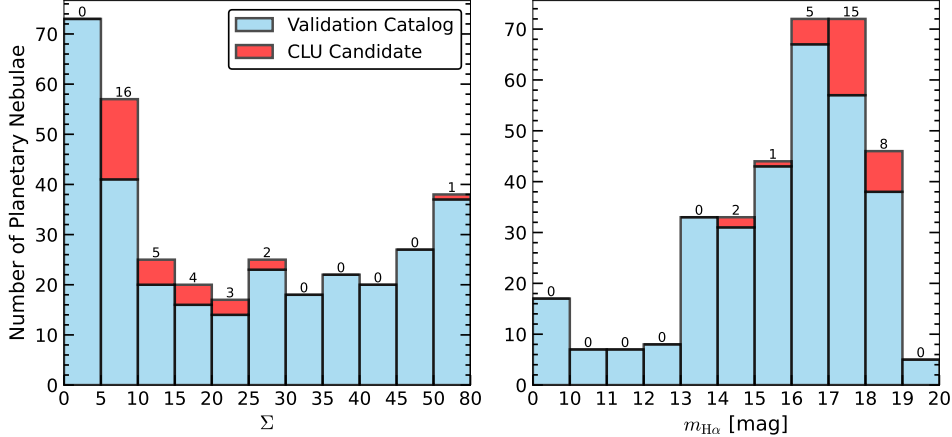


Figure 8. Histogram of True planetary nebula candidates in the validation catalog and PN candidates from our preliminary search on CLU, with respect to different color sigma (Σ ; left panel) and $H\alpha 1$ magnitude ($m_{H\alpha}$; right panel). The blue bars represent sources in the validation catalog, while the red bars represent our candidates. The numbers atop of each bar represent the counts for CLU PN candidates.

tified as other astrophysical objects (e.g., Milky Way H II regions, galaxies, red stars, etc.).

4.2. Planetary Nebula Candidates

After candidate selection and contaminant removal, we finally uncover 31 PN candidates in $|b| < 2^\circ$ and $25^\circ < l < 75^\circ$ of the CLU-FPstack catalog. We illustrate the spatial distribution of the sources in Galactic coordinates in Figure 1, and summarize the notes and respective coordinates of those PN candidates in Table 2.

During the visual inspection, we distinguish the PN candidates and label them with the classification grades (c.f. Section 3.3) based on the visibility of its morphology, as presented in Column (6) of the table. In brief, grade A sources exhibit very clear and distinct morphological features by eye, whereas grade B represents more ambiguous sources that need adjusting the visualization parameters of CLU images to make it visible. Since we are searching for PNe rather than recovering previous work, we are not able to discern the unclear C, needless to say D, sources without references. Among the candidates, 19 (61%) are grade A with clear morphology, and 12 are grade B with only visible morphology after tuning the CLU image. Apart from the clearness of morphology, we also record the references and additional information on its goodness of morphology. We could infer from notes in Column (7) that 12 (39%) candidates are compact and also likely to be stars, and that 4 (13%) are very diffuse and likely to be Galactic H II regions, leaving the rest 15 candidates that do not share similarities with possible contaminants. However, the 31 candidates have all passed our contaminant removal procedure, which means that all sources may be considered as PN candidates.

For references from previous work, 19 of our 31 candidates are reported in other studies initially as PN candidates as well (Parker et al. 2006a; Sánchez Contreras et al. 2008; Viironen et al. 2009a,b; Sabin et al. 2014; Froebrich et al. 2015; Irabor et al. 2018; Kuhn et al. 2021), whereas the remaining 12 sources are newly identified. Within the 19 known sources, 10 of them are suspect PNe, 2 are actually the bright parts of discovered True PNe documented in HASH, 3 are as likely to be PNe as alternative contaminants, 3 are not suggested to be PN by HASH, and 1 appears as a young stellar object (YSO) candidate on SIMBAD. Merely limiting to the new candidates, 5 of them have rather clear morphology (i.e., grade A source), which have our highest confidence to be real PNe. Nevertheless, spectroscopic follow-up on our candidates will serve as the necessary final step for the confirmation of their identity, which we generally leave for future work.

In Figure 8, we plot the distribution of Σ and $H\alpha 1$ magnitude for both True PNe in the validation catalog and candidates from our preliminary search. From the plot, we see effects of catalog search cuts to the property distribution of CLU candidate. In the left panel, we plot the distribution in Σ space, where no CLU sources are detected with $\Sigma < 5$ as expected. Even though 73 of 317 True cataloged PNe have $\Sigma < 5$, the rest 77% in the catalog still have a larger color excess, indicating that using the Σ -based catalog search can indeed find new True PNe. Such sources will exist in our preliminary search candidates and the future CLU PNe catalog. In the right panel, the distribution is demonstrated for the $H\alpha$ magnitude space, where no CLU candidates locate in $m_{H\alpha} < 11$ or beyond the 19.1 magnitude limit of CLU. The peak of the CLU candidates from our preliminary

catalog search are on the fainter end of the distribution, i.e., 1 magnitude dimmer than the validation sources, which indicates that our catalog search will likely find fainter candidates that are more likely to be omitted by visual inspections in previous work.

4.3. Follow-up Spectroscopic Observations

Detection in H α is usually not enough to classify an object as a PN and requires spectroscopic follow-up. We are in the process of obtaining spectroscopic data for several of the candidates for appropriate classification. Here, we present some initial results: low-resolution optical spectroscopic observations of six candidates (from Table 2). The sample selection is performed based on the H α morphology of the object, its position in diagnostic diagrams (like Figure 7), and/or detection in other wavelengths, for example infrared (IR) detection in WISE. A more complete study will be presented in a future work.

The observations were performed using the DouBle SPectrograph (DBSP; Oke & Gunn 1982) attached to the Cassegrain focus of the Palomar 200-inch Hale Telescope. We use the D55 dichroic, the 600 line mm $^{-1}$ grating for the blue arm blazed at 3780 Å, and the 316 line mm $^{-1}$ grating for the red arm blazed at 7150 Å. We use grating angles of 27°17' and 24°38' for the blue and red sides, respectively. With these setups and a slit width of 1.5'' long-slit, we achieve resolving powers of $R = 1600$ in the blue arm and $R = 1400$ in the red arm. This setup provide continuous spectral coverage across 2900–10800 Å, with the division between blue and red arms typically occurring around 5650 Å. The standard star Feige 110 is used for flux calibration.

The standard PypeIt (Prochaska et al. 2020a,b) based optimal-reduction pipeline for DBSP spectra, DBSP_DRP (Roberson et al. 2021), was often seen to be masking bright and extended emission lines, rendering it unsuitable for PNe. Thus, we manually run PypeIt to perform the reduction. We follow the PypeIt recommendations for bright emission lines, and set the parameters `use_2dmodel_mask = False` and `no_local_sky = True`, to avoid masking and local subtraction of the lines. We perform a careful cosmic ray rejection on the two-dimensional spectra using `lacosmic` (van Dokkum 2001), ensuring that none of the emission lines are rejected. We then perform manual trace identification on the two-dimensional spectrum. We use a trace width of six pixels in the spatial direction to obtain the one-dimensional spectrum. We make sure that the extended emission lines are not affected during background subtraction. Owing to the contamination of the one-dimensional spectra from residual cosmic rays, we

closely refer to the two-dimensional spectra while identifying emission lines. For the purpose of this work, only the most prominent emission lines are identified. We discuss the spectral properties of the objects briefly in the following paragraphs. The spectra, along with the CLU images are provided in Appendix B (Figure B1).

CLU J183648.44–064442.8: This object does not have any prior identification/reference. It is an extended source, with a major diameter (D_{maj}) of 18''. Interestingly, the apparent H α morphology resembles that of a bow shock, though sufficient data is not available in favor of or against this scenario. The spectrum is dominated by nebular emission lines; no stellar continuum is detected. The emission lines identified in the spectrum are the first three lines in the Balmer series (H α , β , γ , with the last one being very weak) and the forbidden emission lines of [O II] 3727, 3729 Å, [N II] 6548, 6583 Å, [S II] 6716, 6737 Å, and [S III] 9062, 9532 Å. Interestingly, the spectrum lacks [O III] lines. Such a feature is often attributed to young and very low excitation (VLE) PN. However, the simultaneous presence of the high excitation [S III] lines is puzzling. Strong [S III] with only faint emission features in the blue are often seen in highly reddened PNe (see for example Jacoby & Van de Steene 2004; Fragkou et al. 2018). This may be a low excitation PN where [O III] lines are intrinsically weak, which got further weakened (and, thus, undetected) with reddening. Using the line ratio of H α to H β (Balmer Decrement, BD $_{\alpha\beta}$), and using $E_{B-V} \approx 1.9 \log(\text{BD}_{\alpha\beta}/2.8)$, we get $E_{B-V} \approx 0.94$, which is indeed quite high. Very low excitation (VLE) PNe usually are young and have high densities. For this object, however, we obtain a [S II] 6716 Å/6737 Å line intensity ratio of ~ 1.15 , which, for reasonable temperatures, correspond to low electron densities $n_e \lesssim 500 \text{ cm}^{-3}$ (Osterbrock & Ferland 2006), contrary to our expectation. We further investigate the position of this object in the log(H α /[N II]) – log(H α /[S II]) space (Frew & Parker 2010). We obtain log(H α /[N II]) = 0.046 and log(H α /[S II]) = 0.175. This places the object on the margin between SNRs and PNe. We note here that the neighborhood of this object has significant nebulosity. Several other localized emissions (of varying morphology) are also visible in the Pan-Starrs image. This object may not be PN but simply a denser part of a much larger ionized ISM/SNR. Further observations are needed to understand this candidate better.

CLU J184324.79–014319.2: This is an unresolved point source in the CLU H α image. The spectrum shows a clear signature of a late-type star in the red, with H α . Overall, the spectrum closely resembles that of a symbiotic system (SySt) or a cataclysmic variable (CV). The

accreting white dwarf is possibly too faint to be detected in the blue spectrum. This object, thus, can be considered a false positive.

CLU J192710.49+162128.6: This is also an unresolved point source. It has previously appeared in the list of IPHAS candidate PN in (Viironen et al. 2009b) and remains listed among “New Candidates” in the HASH catalog. Prior to this work, no spectroscopic observation of this object was available. Our spectrum lacks a lot of features except the Balmer series. An emission signature at the [O I] 7774 Å triplet is evident. However, it is unclear whether this is a true feature or a cosmic-ray artifact. The spectrum, overall, is not conclusive. Without the presence of high excitation lines like [O III], the object remains a candidate for compact VLE PN. However, it can also be a false-positive, like an emission-line star.

CLU J194817.60+242116.7: This is again an unresolved point source. It appears as a YSO candidate on SIMBAD from Kuhn et al. (2021). The spectrum, however, shows the signature of a late-type star in the red. Furthermore, it shows the Balmer and Ca II H, K, 8498, 8542, 8662 Å emission lines. These are typical features of a SySt or CV, making this object another false positive.

CLU J194804.17+254848.6: This is a compact but extended source in H α , with a D_{maj} of 9'' in the CLU image. The object appears among extended H₂ sources in Froebrich et al. (2015) and as a PN candidate in Jones et al. (2018) through near-IR K-band spectroscopy. The object also appears among “New Candidates” in HASH. The spectrum shows several emission lines, the prominent ones being: H α , β ; [O III] 5007, 4959 Å; [S II] 6716, 6737 Å; [N II] 6548, 6583 Å; [S III] 9069, 9532 Å; and [O I] 3727, 3729 Å. All of these lines are typical of PNe. The spectrum also appears to show a stellar continuum with absorption features. However, we suspect that this is from an unrelated field star. We obtain log(H α /[N II]) = -0.064 and log(H α /[S II]) = 0.23. Similar to CLU J183648.44–064442.8, this places the object again very close to the margin between PNe and SNRs/H II regions in the diagnostic diagram. With [O III] lines present, we perform a second test with the diagnostic space of log([O III] 5007 Å/H β) – log([N II] 6584 Å/H α) (Figure 5 in Frew & Parker 2010). We obtain log([O III] 5007 Å/H β) = 0.59 and log([N II] 6584 Å/H α) = -0.05. This is consistent with the object being PN, but the possibility of it being an SNR cannot be ruled out. We also obtain a [S II] 6716 Å/6737 Å line intensity ratio of ~1.2, which corresponds to $n_e \lesssim 500 \text{ cm}^{-3}$. We obtain BD $_{\alpha\beta}$ = 10.03,

which leads to a high reddening of $E_{B-V} = 1.1$. Though further observations and analyses are needed to confirm the nature of this object, it stands as a good candidate for a True PN.

CLU J201756.61+335718.2: This is another compact but extended H α source, with $D_{\text{maj}} = 12''$ in the CLU image. A star at the location of the nebula is detected in PS1, which can be the central star. It is also a *Gaia* source with $G=20.7$ and $G_{\text{BP}} - G_{\text{RP}} = 0.74$, but without any reliable parallax information. The nebula is reported by the amateur community. It is currently listed as a Possible PN in HASH with a very low S/N spectrum, with a need for a higher-quality spectrum mentioned. The spectrum shows emission lines typical of PNe: H α , β ; [O III] 5007, 4959 Å, [S II] 6716, 6737 Å, [N II] 6548, 6583 Å, and [O I] 3727, 3729 Å. We perform the same diagnostics as CLU J194804.17+254848.6. We obtain log(H α /[N II]) = 0.033 and log(H α /[S II]) = 0.594. This is consistent with the object being a PN, but it is also close to the spaces for SNR/H II. Additionally, we get log([O III] 5007 Å/H β) = 0.579 and log([N II] 6584 Å/H α) = -0.149. In this space, the object lies away from the crowd of either SNR or H II regions, and appears more consistent with being a PN. We obtain a [S II] 6716 Å/6737 Å line intensity ratio of ~1.18, which again corresponds to $n_e \lesssim 500 \text{ cm}^{-3}$. The object, however, does not appear to be as severely reddened. We obtain BD $_{\alpha\beta}$ = 4.28, which leads to a moderate reddening of $E_{B-V} = 0.34$. Overall, the object stands as a strong candidate for a True PN.

Table 2. Thirty-One Planetary Nebula Candidates from the Preliminary Search

Name	R.A. (J2000)	Decl. (J2000)	<i>l</i>	<i>b</i>	Grade	Notes
(1)	(2) (°) (°)	(3) (°) (°)	(4) (°)	(5) (°)	(6)	(7)
CLU J183648.44–064442.8	279.20195	–6.74537	25.26449	0.16175	A	Diffuse, also possibly an HII region; clear morphology
CLU J184312.04–044522.6	280.80017	–4.75628	27.76107	–0.34024	B	Red star or PN; visible morphology
CLU J184324.79–014319.2	280.85328	–1.72201	30.48428	0.99928	A	Faint & compact; clear morphology
CLU J184443.03–030355.8	281.17928	–3.06551	29.43786	0.09585	B	Masked in an epoch; inconclusive with a bright star in the FoV
CLU J184932.49–004429.9	282.38538	–0.74163	32.05557	0.08374	A	Very diffuse, also possibly an HII region; clear morphology in FoV of 150"
CLU J193948.71+203344.0	294.95297	20.56221	56.63976	–0.82667	B	Milky Way H II region or PN; visible morphology
CLU J194130.75+215650.2	295.37815	21.94729	58.03997	–0.48734	B	Compact, also possibly a star; visible morphology
CLU J194224.54+232009.7	295.60226	23.33603	59.34859	0.02151	B	Compact, also possibly a star; visible morphology
CLU J194302.30+233615.4	295.75959	23.60428	59.65308	0.02958	B	Faint & compact, also possibly a star; visible morphology
CLU J194816.04+254227.7	297.06684	25.70769	62.06862	0.05648	A	Compact, also possibly a star; clear morphology
CLU J200514.13+322139.7	301.30889	32.36103	69.67817	0.35278	B	PN or symbiotic star, also likely a jet component of IRAS 20032+3212
CLU J200617.44+334335.9	301.57267	33.72664	70.94905	0.89943	A	Compact, also possibly a star; clear morphology
CLU J184355.71–023220.2	280.98211	–2.53894	29.81633	0.51156	A	Part of a True PN (R.A.= 280.9871, Decl.= –2.5356, Parker et al. 2006a)
CLU J184505.23+001158.6	281.27181	0.19961	32.38552	1.50401	A	None PN suspected in HASH (Viironen et al. 2009b) with low S/N spectrum
CLU J191233.22+114631.3	288.13844	11.77535	45.80034	0.73884	A	Asymptotic giant branch star suspected in HASH (Viironen et al. 2009a)
CLU J191614.08+125202.2	289.05872	12.86728	47.18501	0.44987	A	Studied by Froebrich et al. (2015) and Jones et al. (2018); clear morphology
CLU J191713.48+141747.2	289.30615	14.29645	48.56155	0.9035	B	Suspected PN in SIMBAD reported by Irabor et al. (2018); visible morphology
CLU J192140.59+155353.8	290.41919	15.89823	50.48032	0.70474	A	Symbiotic Star or young PN in HASH (Sabin et al. 2014); clear morphology
CLU J192710.49+162128.6	291.79372	16.35794	51.51049	–0.24058	A	Compact, reported by Viironen et al. (2009b); clear morphology
CLU J192802.95+171643.3	292.01229	17.27869	52.41955	0.01468	B	None PN suspected in HASH (Viironen et al. 2009a) without spectrum
CLU J193719.79+202112.4	294.33225	20.35345	56.17254	–0.42261	A	Part of a True PN (R.A.= 294.3278, Decl.= 20.3508, Sabin et al. 2014)
CLU J194804.17+254848.6	297.01736	25.83551	62.13741	0.14842	A	Diffuse, reported by Froebrich et al. (2015); clear morphology
CLU J194817.60+242116.7	298.12297	28.79328	65.2025	0.81912	B	Reported by Viironen et al. (2009b); visible morphology
CLU J195229.51+284735.8	298.12733	24.35465	60.90422	–0.63268	A	Compact, young stellar object candidate in SIMBAD (Kuhn et al. 2021)
CLU J195405.86+280740.6	298.52444	28.12795	64.81316	0.1744	A	PN in SIMBAD reported by Sánchez Contreras et al. (2008); clear morphology
CLU J195707.62+303215.8	299.28175	30.53773	67.21649	0.85807	B	Mid-infrared source in SIMBAD, unlabeled in HASH; visible morphology
CLU J195956.42+304823.9	299.98508	30.80663	67.7622	0.48326	A	Reported by Viironen et al. (2009a) without spectrum; SNR G067.8+0.5 nearby
CLU J200514.60+322125.1	301.31082	32.35697	69.67561	0.34923	A	Young PN (Viironen et al. 2009a; Corradi et al. 2010); clear morphology
CLU J200850.35+333729.9	302.20978	33.6249	71.14999	0.39835	B	Suspected star forming region in SIMBAD; visible morphology
CLU J201126.21+331606.7	302.85921	33.26853	71.14701	–0.25021	A	None PN suspected in HASH (Viironen et al. 2009a) without spectrum
CLU J201756.61+335718.2	304.48587	33.95506	72.46988	–0.99632	A	Extended, Possible PN reported by the amateur community

NOTE— Col. (1): Name of the object in the CLU survey. Col. (2)–(5): Coordinates. Col. (6): Grade of the source assigned

5. DISCUSSION

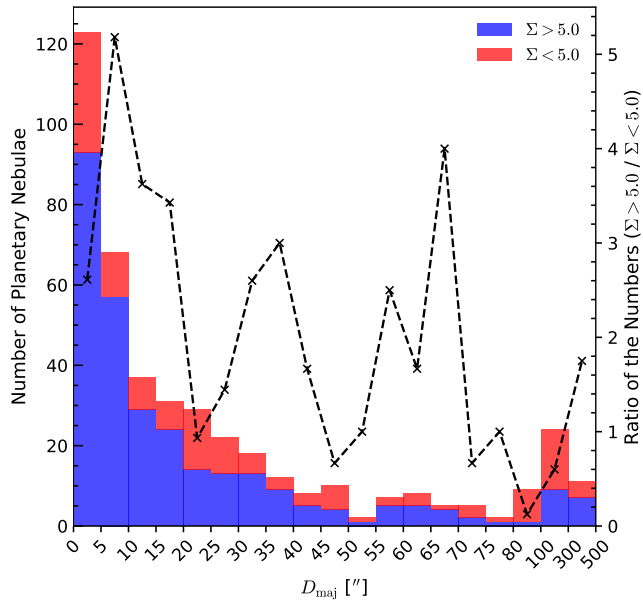


Figure 9. Stacked histogram of planetary nebulae in the validation catalog with respect to different major diameters (D_{maj}). The crosses show the number ratio of candidates with $\Sigma > 5$ to $\Sigma < 5$. Sources are divided into two groups with color sigma larger or smaller than 5.

5.1. Caveats

We note three primary caveats that are inherent in our methodology of source catalog search. First, our search for PNe focuses on H α excess and necessitates a minimum $m_{\text{H}\alpha}$ threshold of 11, leading to the exclusion of those very bright nebulosities from consideration. Nonetheless, $m_{\text{H}\alpha} = 11$ is a rather bright limit, and the majority of the brightest PNe are very likely to have already been discovered and studied.

Second, the photometric calculations employ an aperture size of only 5 pixels ($\sim 5''$) which can lead to a possible underestimation of the color sigma because a portion of the nebular emission may not be captured. In Figure 6, 32% objects in the validation catalog have Σ smaller than 5. Interestingly, larger D_{maj} sources are in the $\Sigma < 5$ group, whereas sources with $\Sigma > 5$ are distributed more frequently with smaller D_{maj} , as shown in Figure 9. It is reasonable to consider using a larger aperture, but contaminating emission from nearby sources may bias the detectability of the emission line signal. Alternatively, lowering the Σ thresholds has the risk of directly including more contaminants. If the contaminant removal techniques matures, we may adopt a lower requirement for Σ (2.5 to 3) that still holds as a useful H α excess indicator. However, a bright subpart of

the nebulae should be sufficient to be picked during our catalog searches, which will lead to subsequent visual inspections with zoomed-out, large FoV images for further selection.

Finally, another issue on the large PNe is that their optical center encoded in PS1 and H α center from the CLU may not coincide, with $dist2stack$ easily exceeding our current cut-off value of $1.5''$. But, previous systematic searches that relied on visual scrutiny are sensitive to large PNe, as exemplified by Sabin et al. (2014) on rebinned H $\alpha - r$ difference images. Consequently, it is unlikely that there are large numbers, or any, large PNe left to be discovered. In our preliminary search, most discovered candidates are indeed compact and star-like as expected (c.f. Column (7) of Table 2).

For stellar population removal (c.f. Section 4.1.2), our current cuts on the $(r - \text{H}\alpha)$ versus $(r - i)$ diagram provides only a rough solution. Viironen et al. (2009a) applied similar cuts to initially identify thousands of PN candidates from the IPHAS images. Nevertheless, subsequent spectroscopic follow-up revealed that over 80% of these sources were still emission-line stars, which underscored the similarities in photometric properties between compact PNe and stars whereby a more reliable stellar population removal would be a difficult task. In fact, young PNe or pre-PN could be relatively red, and dust obscured sources may also be reddened, both of which add to false positives. In our preliminary search, we estimate to effectively remove $\sim 90\%$ of stars with our simple criterion. Yet, since stars roughly take up to 48% of those 10^4 candidate sources from the source catalog search, the remaining number of stars ($48\% \times (100\% - 90\%) = 5\%$) is still more than 15 times the number of PN candidates (0.3%). In the future, we will improve and expand these color-color cuts to filter more stars while keeping the red PNe.

For further removal, mid-IR (MIR) and radio properties could be of help (e.g., Parker et al. 2012). Since genuine PNe exhibit bremsstrahlung emission, Condon et al. (1999) utilized the 1.4 GHz NRAO VLA Sky Survey (NVSS; Condon et al. 1998) images to identify PNe over radio-quiet MIR contaminants with the criterion of $S(25\mu\text{m}) \gtrsim 2.5\text{ mJy beam}^{-1}$ by positional coincidence for a 4% of missing rate, demonstrating that radio selection would aid on to reliable detection of PNe. Meanwhile, as adopted by HASH, the median $8\mu\text{m}$ MIR to radio flux ratio should be consistent with 4.7 ± 1.1 for all PNe (Cohen et al. 2011). In addition, WISE could be used with all-sky coverage, which may help distinguishing symbiotic stars, post asymptotic giant branch stars, Wolf-Rayet shells, Mira variables and other red stars (e.g., Parker et al. 2012; Akras et al. 2019). Similar to

the H α -PS1 color-color cut, we briefly show the potential of WISE color cuts here. Generally, (W1 – W2), (W2 – W3), and (W1 – W4) can all separate PN candidates from stars (e.g., Parker et al. 2012; Akras et al. 2019). If we adopt a very rough cut off with W1 – W2 < 0 and W2 – W3 < 1 and W1 – W4 < 2, 91% stars are removed while 61% PN candidates are kept; whereas 88% in the validation catalog remain, since they are more extended with presumably less similarity to stars. We plot sources from the validation catalog and our preliminary search with their (W1 – W2) versus (W2 – W3) in Figure 10 for demonstration.

Additionally, we believe a future systematic search for PNe may involve adopting a more modern and reliable detection method, such as machine learning (e.g., recent attempts by Sun et al. 2024), to remove all contaminants directly from candidate lists and finalize the PN candidates for spectroscopic follow-up. However, feature engineering for a machine learning classifier is complex, requiring well-established empirical expressions based on physical properties of the sources². With prospective homogeneous sampling, the future CLU PN catalog can serve as a labeled validation dataset for emerging machine learning techniques.

Finally, we reiterate that all sources documented from the preliminary search and any catalog search of the same kind should only be considered as candidates. In general, the cuts in source catalog searches only filter out apparent emission-line excess objects that are not overly extended or bright, encompassing candidates such as some Strömgren spheres, compact H II regions, Wolf-Rayet shells, SNRs, nearby emission-line galaxies, stars, image artifacts, and finally compact young PNe. Visual scrutiny is always needed to identify PN candidates, where better contaminant removal techniques will be essential to reduce the labor and boost its efficiency. Typical visual inspection can reliably discern artifacts, most Milky Way H II regions, and several compact stellar signals. Automatic artifact removal methods are also readily developed (e.g., van Dokkum 2001), e.g., for images having sufficient quality like those with more than three images going into the stack for a single source location (Cook et al. 2024, submitted; Zhang et al. 2024, submitted). Nevertheless, spectroscopic follow-up is also indispensable for establishing a high-fidelity sample. For spectral features, H II regions usually exhibit [N II]/H α ratios below 0.5 to 0.7 (Kennicutt et al. 2000), while non-obscured PNe tend to display higher ratios indicative of

elevated gas temperatures. Bright MIR emission characterizes Wolf-Rayet shells, enabling their identification via WISE all-sky fluxes. SNRs are identifiable by their prominent sulfur and oxygen lines. Optical spectroscopy facilitates finding galaxies through their redshifted emission lines. In future work, we will propose spectroscopic follow-up for all PN candidates to confirm their status.

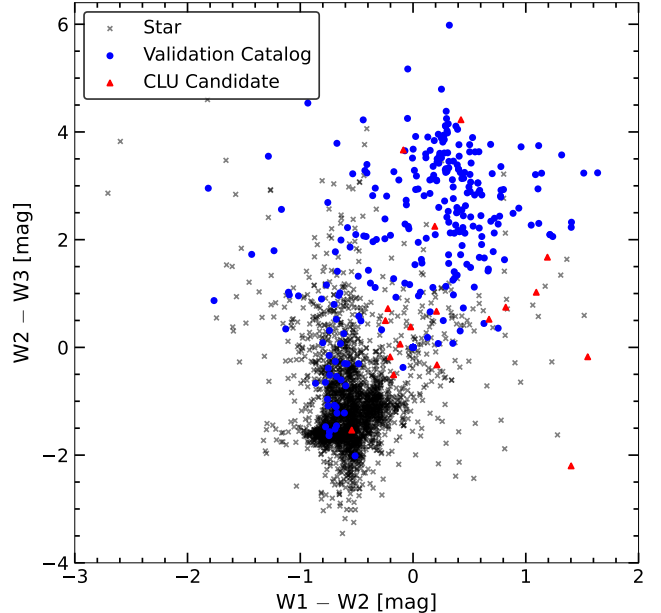


Figure 10. An example color-color diagram depicting the WISE (W2 – W3) versus (W1 – W2) scatter plot of labelled stars from contaminant removal, planetary nebula candidates in the validation catalog, and candidates from our preliminary search on CLU.

5.2. Prospects for the CLU Catalog of New Planetary Nebula

The known Galactic PN population is as large as $\sim 3,900$, which is, nevertheless, below the predicted value. Depending on the formation scheme of PNe, if a more strict case (e.g., close binaries forming a common-envelope phase) is required, a theoretical value of $\sim 6,600$ (De Marco & Moe 2005) should be expected. However, it is largely accepted that a mere 10–20% of all PNe have binary CSPN (Miszalski et al. 2009), and thus, the overall number of Galactic PNe can be up to $46,000 \pm 13,000$ based on a stellar population synthesis model (Moe & De Marco 2006). Hence, the true number of Galactic PNe also provides a test of current demographic model for stars in our Galaxy.

Previous surveys of PNe (e.g., Abell 1966; Perek & Kohoutek 1967; Acker et al. 1992; Parker et al. 2005, 2006a; Miszalski et al. 2008; Boumis et al. 2006; Górný 2006;

² Although deep learning methods (see e.g., review by LeCun et al. 2015) do not require feature engineering, the interpretability of deep neural networks remains challenging.

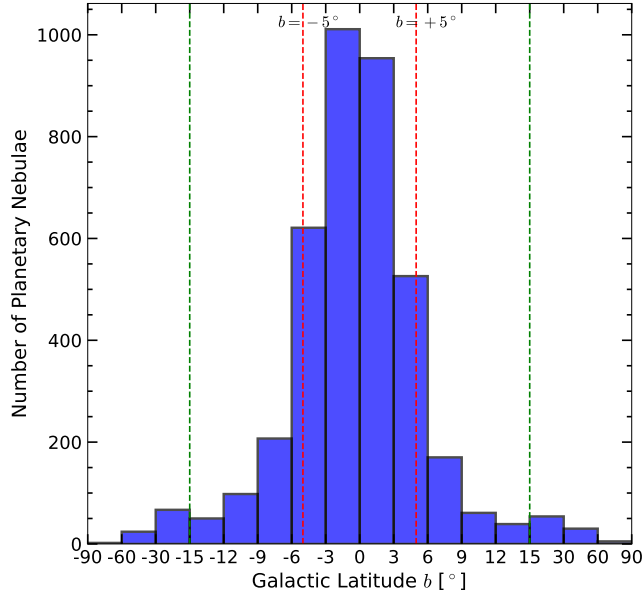


Figure 11. Histogram of the Galactic latitudes of the True, Likely, and Possible Galactic planetary nebulae in the HASH database. The bins for the latitudes are not evenly spaced.

(Viironen et al. 2009a,b; Sabin et al. 2014) made significant advancements in finding thousands of PNe with considerable effort at lower galactic latitudes, where the largest number of PNe are likely to be found. In addition, the amateur community has made considerable contributions to the search for PNe in other parts of the sky (e.g., Kronberger et al. 2012, 2014, 2016; Acker & Le Dù 2014; Le Dù 2017; Le Dù et al. 2022). We aim for the CLU survey to complement these previous efforts via systematic PNe searches in our survey area, where we anticipate the largest contributions to come from intermediate Galactic latitudes.

The largest Galactic plane survey in the northern hemisphere – IPHAS – was limited to $|b| \leq 5^\circ$, with an exclusive focus of revealing emitters near the highly obscuring Galactic plane. SHS, the largest Galactic plane search for PNe in the southern hemisphere, has a coverage of $-145^\circ < l < 30^\circ$ and mainly $|b| < 6^\circ$ with substantial coverage extending to $b = 15^\circ$. According to Parker et al. (2006a) and Miszalski et al. (2008), the number of SHS/MASH PNe at $|b| > 5^\circ$ declines significantly comparing to the number of PNe within $|b| = 5^\circ$ (~ 1000). Yet with a detection limit down to $\sim 10^{-16} - 10^{-17}$ erg s $^{-1}$ cm $^{-2}$, ~ 200 PNe are still discovered by SHS between $5^\circ < |b| < 10^\circ$, and ~ 20 PNe are discovered between $10^\circ < |b| < 15^\circ$. Therefore, we can expect plenty of new PNe to be discovered between $5^\circ < b < 15^\circ$, assuming that the distribution of actual PNe is close to that of the discovered population.

Since SHS was conducted on $\sim 4,000$ deg 2 of the Southern Milky Way (Parker et al. 2005), and since CLU covers an area of 3,400 deg 2 near Galactic Plane outside of both IPHAS and SHS, we anticipate finding around $220/4000 \times 3400 = 187$ new PNe, even though SHS covers more of the Galactic bulge which may be riper for PNe with higher areal number density. Moreover, we are also likely to find a few new PNe at higher galactic latitudes. If we further refer to the HASH database (see Figure 11), $\sim 1/3$ of known PNe are located beyond $|b| = 5^\circ$, and specifically 5% of PNe are at $|b| > 15^\circ$. Thus, we may expect to find roughly $187 \times 0.05/(0.33 - 0.05) = 35$ high latitude PNe. Yet, since the calculation is purely based on the distribution of known PNe, the result of finding a mere 35 high latitude PNe might be underestimated if more PNe are actually distributed slightly higher in some clusters or just solely by itself.

In practice, the lower line sensitivity of CLU might not be compensated by image stacking and careful selection techniques, which could lower the expected numbers of CLU PNe. However, despite of a brighter detection limit of the CLU (1.6×10^{-14} erg s $^{-1}$ cm $^{-2}$, Cook et al. 2024; submitted), we are already finding new candidates in the same fields as those of deeper searches. Meanwhile, the CLU survey will also face a lower contamination level at higher latitudes where the easily removable nearby galaxies could become the major false positive. After the entire catalog search with automatic and visual contaminant removal procedures, we anticipate to find approximately $187 + 35 \approx 220$ new PNe only through scaling by areas. Other practical factors may affect the final number of CLU PNe, which we leave as a topic for future work.

6. CONCLUSION

Planetary nebulae play a pivotal role in deciphering the intricacies of stellar evolution, Galactic chemical enrichment, and broader cosmological phenomena. Leveraging data from the CLU narrowband H α emission-line galaxy survey, our project aims to systematically detect and catalog PNe within the CLU survey extending above a declination of -20° .

Originally targeting H α galaxies, the CLU survey has proven its efficacy in PN searches with a 98% recovery rate of 441 PNe within a validation catalog constructed from IPHAS/HASH data. The quality and utility of CLU were shown by the fact that 90% of these sources exhibit readily discernible morphology in CLU-H α images. Notably, our recovery rates remained consistently high across sources of all HASH PN classes, with 95% of

True, 71% of Likely, and 81% of Possible sources being readily identified.

We conducted a preliminary search for PN candidates, employing a source catalog search primarily based on color sigma ($\Sigma > 5$) supplemented by visual inspection for contaminant removal. Within the region of $|b| < 2^\circ$ and $25^\circ < l < 75^\circ$, we discovered 31 PN candidates where 12 are new sources that have not appeared in any previous studies. Spectroscopic follow-up has been conducted for six candidates so far, revealing that four of them are good candidates and two of them are likely contaminants.

Spanning intermediate to high Galactic latitudes, the CLU survey presents a unique opportunity for uncovering PNe in previously unexplored regions of the sky. Looking ahead, our future work will be geared towards refining catalog search criteria and conducting spectroscopic follow-up to validate and confirm additional candidates.

ACKNOWLEDGMENTS

We thank the anonymous referee for helpful suggestions. R.D. thanks Luis C. Ho and Yuanze Ding for useful suggestions in the early stage of the project. S.B. thanks Howard E. Bond for useful discussion on the DBSP spectra of the planetary nebula candidates.

We make use of the Intermediate Palomar Transient Factory project which is a scientific collaboration among the California Institute of Technology, Los Alamos National Laboratory, the University of Wisconsin, Milwaukee, the Oskar Klein Center, the Weizmann Institute of Science, the TANGO Program of the University System of Taiwan, and the Kavli Institute for the Physics and Mathematics of the Universe.

This research has made use of the HASH PN database at hashpn.space. The HASH database is maintained by the Laboratory for Space Research at the University of Hong Kong.

This research has made use of the SIMBAD database, operated at CDS, Strasbourg, France. This research has made use of the NASA/IPAC Extra-galactic Database (NED), which is operated by the Jet Propulsion Laboratory, California Institute of Technology, under contract with the National Aeronautics and Space Administration.

The Pan-STARRS1 Surveys (PS1) and the PS1 public science archive have been made possible through contributions by the Institute for Astronomy, the University

of Hawaii, the Pan-STARRS Project Office, the Max-Planck Society and its participating institutes, the Max Planck Institute for Astronomy, Heidelberg and the Max Planck Institute for Extra-terrestrial Physics, Garching, Johns Hopkins University, Durham University, the University of Edinburgh, the Queen's University Belfast, the Harvard-Smithsonian Center for Astrophysics, the Las Cumbres Observatory Global Telescope Network Inc., the National Central University of Taiwan, the Space Telescope Science Institute, the National Aeronautics and Space Administration under grant no. NNX08AR22G issued through the Planetary Science Division of the NASA Science Mission Directorate, the National Science Foundation Grant no. AST-1238877, the University of Maryland, Eotvos Lorand University (ELTE), the Los Alamos National Laboratory, and the Gordon and Betty Moore Foundation.

Funding for SDSS-III has been provided by the Alfred P. Sloan Foundation, the Participating Institutions, the National Science Foundation, and the U.S. Department of Energy Office of Science. The SDSS-III website is <http://www.sdss3.org/>. SDSS-III is managed by the Astrophysical Research Consortium for the Participating Institutions of the SDSS-III Collaboration, including the University of Arizona, the Brazilian Participation Group, Brookhaven National Laboratory, Carnegie Mellon University, the University of Florida, the French Participation Group, the German Participation Group, Harvard University, the Instituto de Astrofisica de Canarias, the Michigan State/Notre Dame/JINA Participation Group, Johns Hopkins University, Lawrence Berkeley National Laboratory, Max Planck Institute for Astrophysics, Max Planck Institute for Extraterrestrial Physics, New Mexico State University, New York University, Ohio State University, Pennsylvania State University, the University of Portsmouth, Princeton University, the Spanish Participation Group, the University of Tokyo, the University of Utah, Vanderbilt University, the University of Virginia, the University of Washington, and Yale University.

Facilities: 48-inch Oschin, 2.5 m INT, 200-inch Hale

Software: ASTROPY (Astropy Collaboration et al. 2013, 2018, 2022), MATPLOTLIB (Hunter 2007), NUMPY (van der Walt et al. 2011; Harris et al. 2020), SCIENCEPLOTS (Garrett 2021), TOPCAT (Taylor 2005)

APPENDIX

A. RECOVERY RESULTS OF THE IPHAS CATALOG

In Section 3, we discussed the visual recovery process applied to a validation catalog constructed from IPHAS/HASH data. Table A1 presents our grading in Column (9) and observational notes for each candidate in Column (10), as well as detailed information for each source collected from previous surveys.

B. DBSP SPECTRA OF SIX PN CANDIDATES

We provide the DBSP optical spectroscopic observations of the six PN candidates. In all the Figures, the upper and lower left panels show the CLU H α 1 “On” and H α 2 “Off” filter images, respectively. The upper middle and right panels show the two-dimensional spectra from DBSP in the blue and red channels respectively. The lower right panel shows the one-dimensional spectrum extracted from the marked trace. The unreliable (elevated noise, prominent cosmic rays etc.) regions of the spectrum have been shaded.

Table A1. Results of Recovering the IPHAS PNe in the CLU Imaging Data

Name	R. A. (J2000) (h m s)	Decl. (J2000) (° ' '')	D_{maj} (")	D_{min} (")	M. Mor.	S. Mor.	Class	Grade	Notes	l (°)	b (°)	Ref.
(1)	(2)	(3)	(4)	(5)	(6)	(7)	(8)	(9)	(10)	(11)	(12)	(13)
PM 1-246	18 36 02.4	-00 02 27.1	16	16	E		L	C		31.13806	3.40687	1
PM 1-262	18 53 02.0	+06 44 15.3			S	T	A			39.11395	2.71376	1
PM 2-40	19 17 50.6	+08 15 08.3			R		L	A		43.28616	-2.0518	1
PM 1-302	19 27 51.4	+14 01 27.8	10		R	ars	T	A		49.5371	-1.49728	1
PM 1-305	19 31 41.3	+22 43 38.8	15		E	as	T	A		57.61212	1.87629	1
PM 1-319	20 10 37.7	+31 37 56.6			S		L	A		69.68419	-1.00291	1
PM 1-332	21 34 23.2	+52 37 27.6	6.5	5.7	E		T	A		95.54608	0.56095	1
BV 5-1	00 19 58.7	+62 59 01.7	42	10	B	ms	T	A		119.368	0.32993	2
We 1-1	00 38 54.0	+66 23 49.3	22	20	E	ars	T	A	Band 2 Brighter Than 1	121.67507	3.55588	2
K 3-90	01 24 58.6	+65 38 36.1	10	9	E	mrs	T	A		126.38442	2.9967	2
We 2-5	01 42 37.9	+60 09 47.2	210	165	B	amrs	T	A		129.26373	-2.07777	2
IC 1747	01 57 35.8	+63 19 18.1	13	13	E	ms	T	A		130.277	1.39738	2
K 3-91	01 58 35.4	+66 34 00.5	10	10	B	ms	T	A		129.549	4.56161	2
K 3-92	02 03 41.3	+64 57 39.1	18	12	B	prs	T	A		130.48392	3.15384	2
K 3-93	02 26 30.0	+65 47 53.3	10	10	B	ars	T	A	Band 2 Brighter Than 1	132.47373	4.70305	2
Sh 2-200	03 10 58.9	+62 47 54.9	360	345	E	amrs	T	A		138.12801	4.11928	2
K 3-94	03 36 08.1	+60 03 46.3	10	7	B	amrs	T	A		142.14967	3.48734	2
M 1-4	03 41 43.4	+52 17 00.3	4.2	4.2	E	mrs	T	A		147.40051	-2.30686	2
M 2-2	04 13 15.0	+56 56 58.1	13		R	amrs	T	A		147.87223	4.19524	2
K 3-64	04 13 27.3	+51 51 00.9	7.5	7.5	E	mrs	T	A		151.40162	0.51129	2
K 3-65	04 15 54.5	+48 49 40.6	7		E		T	A	Flat Continuum; Varying	153.77028	-1.40651	2
K 4-47	04 20 45.3	+56 18 12.6	12.2		B	p	T	A		149.066	4.45202	2
K 3-69	05 41 22.1	+39 15 08.1			S		T	A		170.73981	4.65065	2
M 1-5	05 46 50.0	+24 22 02.9	2.8	2.3	S		T	A		184.04527	-2.14238	2
K 3-70	05 58 45.4	+25 18 43.8	5.5		E	am	T	A		184.60722	0.667	2
K 3-70	05 58 45.4	+25 18 43.8	5.5		E	am	T	A		184.60722	0.667	2

Table A1 *continued*

Table A1 (*continued*)

Name	R. A. (J2000) ($^{\text{h}}\text{m}^{\text{s}}$) (1)	Decl. (J2000) ($^{\circ}\text{'}$ (2))	D_{maj} ($''$) (3)	D_{min} ($''$) (4)	M. Mor. (5)	S. Mor. (6)	Class (7)	Grade (8)	Notes (9)	l ($^{\circ}$) (10)	b ($^{\circ}$) (11)	Ref. (13)
We 1-4	06 14 33.7	+07 34 29.9	41.4	37.6	B	ps	T	A		201.95782	-4.65928	2
K 3-72	06 23 54.9	+05 30 12.9	22.9	18	B	as	T	A		204.88368	-3.57761	2
M 1-6	06 35 45.1	-00 05 37.4	4	2.7	B	mrs	T	A		211.22513	-3.53224	2
M 1-6	06 35 45.1	-00 05 37.4	4	2.7	B	mrs	T	A		211.22513	-3.53224	2
K 4-48	06 39 55.9	+11 06 30.7	4	S			T	A		201.73885	2.52328	2
M 1-8	06 53 33.8	+03 08 26.9	21	16	B	ps	T	A		210.37768	1.90396	2
K 3-6	18 33 17.5	+00 11 47.2	0.7	R			T	A		31.03504	4.12643	2
Abell 47	18 35 22.6	-00 13 49.7	17.5	12.3	B	rs	T	A		30.89317	3.46779	2
PC 20	18 43 03.4	-00 16 37.5	12	5	B		T	A		31.72957	1.7381	2
K 3-13	18 45 24.6	+02 01 23.8		B	s		T	A		34.0465	2.26327	2
HaTr 10	18 50 24.6	-01 40 18.0	32	19.5	B	aprs	T	A		31.32706	-0.53372	2
WeSb 4	18 50 40.3	-01 03 11.2	42	33	B	mps	T	A		31.90733	-0.30973	2
K 3-15	18 51 41.5	+09 54 52.4	2	E			P	A		41.80234	4.44704	2
K 3-17	18 56 18.2	+07 07 26.2	18.6	11.9	B	ms	T	A		39.82761	2.1666	2
M 1-65	18 56 33.6	+10 52 10.1	4.2	4	E	ams	T	A		43.19856	3.81018	2
M 1-66	18 58 26.3	-01 03 45.7	3	3	B	mps	T	A		32.78375	-2.04185	2
K 3-18	19 00 34.8	-02 11 57.6	4	S	m		P	A		32.01485	-3.03618	2
K 3-19	19 01 36.6	-01 19 07.9	10	S			T	A		32.91709	-2.86434	2
K 3-20	19 02 10.2	-01 48 45.3		S			T	A		32.54065	-3.21366	2
NGC 6741	19 02 37.1	-00 26 57.0	9.1	6.5	E	mps	T	A		33.80713	-2.6923	2
HaTr 11	19 02 59.3	+03 02 21.3	21	21	E	ms	T	A		36.95409	-1.1803	2
HaTr 13	19 08 02.1	+02 21 24.3	21	B	s		T	A		36.92501	-2.61319	2
K 3-24	19 12 05.8	+15 09 04.5	12	8	B	mps	T	A		48.74341	2.39845	2
Hen 2-428	19 13 05.5	+15 46 39.4	40	15	B	amrs	T	A		49.41022	2.47518	2
Abell 56	19 13 06.1	+02 52 47.9	206	182	R	mr	T	A		37.9727	-3.49648	2
M 2-47	19 13 34.6	+04 38 04.5	6.9	4.9	E	m	T	A	Band 2 Bigger and Brighter Than 1	39.58645	-2.79202	2
M 1-69	19 13 53.9	+03 37 41.7	9.4	E	T		T	A		38.72967	-3.32794	2
Hen 2-430	19 14 04.1	+17 31 32.5	5	2	B	p	T	A		51.07073	3.07509	2

Table A1 (*continued*)

Table A1 (*continued*)

Name	R. A. (J2000) (^h ^m ^s)	Decl. (J2000) ([◦] [′] [″])	D_{maj}	D_{min}	M. Mor.	S. Mor.	Class	Grade	Notes	l ([◦])	b ([◦])	Ref.
(1)	(2)	(3)	(4)	(5)	(6)	(7)	(8)	(9)	(10)	(11)	(12)	(13)
K 3-26	19 14 39.2	+00 13 36.3	10	B	mps	T	A		35.7879	-5.05958	2	
K 3-29	19 15 30.6	+14 03 49.8	2.5	B		T	A		48.16197	1.16306	2	
K 3-30	19 16 27.7	+05 13 19.4	3	3	R		T	A		-3.15727	2	
K 3-31	19 19 02.6	+19 02 21.0	2	2	S		T	A	52.96189	2.73143	2	
PM 1-295	19 19 18.8	+17 11 48.1	20	R	m	L	A		51.36131	1.81434	2	
M 4-14	19 21 00.7	+07 36 52.4	28	14	B	ps	T	A	43.08853	-3.04356	2	
K 3-33	19 22 26.7	+10 41 21.4	4.5	B		T	A		45.97235	-1.91293	2	
Hen 2-432	19 23 24.8	+21 08 00.5	5	R	am	T	A		55.29547	2.80611	2	
Hen 1-1	19 23 46.9	+21 06 38.2	8	6	B	mps	T	A	55.31566	2.71974	2	
K 3-34	19 24 02.7	+25 18 47.6	12	9.6	B	amps	T	A	59.06268	4.63926	2	
Vy 2-2	19 24 22.2	+09 53 56.3	3.1	2.6	S		T	A	45.49804	-2.70312	2	
Hen 1-2	19 26 37.8	+21 09 27.0	5	5	E	ms	T	A	55.67135	2.15673	2	
K 3-35	19 27 44.0	+21 30 03.8	6	3	B	amps	T	A	56.09617	2.09372	2	
PB 9	19 27 44.8	+10 24 20.8	13	11	E	ams	T	A	46.33878	-3.19541	2	
PB 10	19 28 14.4	+12 19 36.2	11	9	B	mps	T	A	48.08823	-2.38838	2	
K 4-28	19 30 16.7	+14 47 21.8		S		T	A		50.48972	-1.64666	2	
NGC 6803	19 31 16.5	+10 03 21.5	8.2	E		T	A		46.44431	-4.12522	2	
K 4-30	19 33 09.0	+22 58 33.5	R		T	A			57.99246	1.70083	2	
K 3-37	19 33 46.7	+24 32 27.1	2.5	2.5	E		T	A	59.43307	2.33074	2	
K 3-38	19 35 18.4	+17 13 00.7	4	E	ap	T	A		53.19992	-1.5335	2	
K 3-39	19 35 54.4	+24 54 50.0	7	S		T	A		59.99397	2.08883	2	
K 3-40	19 36 21.8	+23 39 47.9	4	E		T	A		58.95171	1.3892	2	
M 1-71	19 36 26.9	+19 42 24.0	6	3.7	E	m	T	A	55.50702	-0.55794	2	
Hen 2-440	19 38 08.4	+25 15 40.7	3	R		T	A		60.54409	1.81714	2	
HuD 1	19 38 52.1	+25 05 32.6	2.1	S		T	A		60.47773	1.59047	2	
K 3-41	19 39 15.9	+16 20 48.5	7.5	6.5	E		T	A	52.90262	-2.78511	2	
K 3-42	19 39 35.8	+20 19 01.9	3.4	S		T	A		56.40163	-0.9034	2	
M 1-73	19 41 09.3	+14 56 59.4	8.8	6	B	ms	T	A	51.90691	-3.86708	2	

Table A1 *continued*

Table A1 (*continued*)

Name	R. A. (J2000) ($^{\text{h}}\text{m}^{\text{s}}$)	Decl. (J2000) ($^{\circ}\text{'}$ $''$)	D_{maj}	D_{min}	M. Mor.	S. Mor.	Class	Grade	Notes	l ($^{\circ}$)	b ($^{\circ}$)	Ref.
(1)	(2)	(3)	(4)	(5)	(6)	(7)	(8)	(9)	(10)	(11)	(12)	(13)
M 1-72	19 41 34.0	+17 45 17.5	4		R	mrs	T	A		54.40078	-2.57156	2
PC 22	19 42 03.5	+13 50 37.4	20	12	B	as	T	A		51.04832	-4.60063	2
Abell 63	19 42 10.3	+17 05 14.4	48	42	B	ps	T	A		53.89099	-3.0267	2
M 1-74	19 42 18.8	+15 09 08.2	5		R	m	T	A		52.22133	-4.01074	2
M 1-74	19 42 18.8	+15 09 08.2	3	3	R	m	T	A		52.22133	-4.01074	2
Hen 2-447	19 45 22.2	+21 20 04.0	3	1.2	B	mps	T	A		57.95452	-1.56969	2
K 3-45	19 46 15.6	+24 11 03.7	7	7	B	s	T	A		60.52362	-0.31834	2
Hen 1-3	19 48 26.4	+22 08 37.3	8	8	E	m	T	A		59.013	-1.7792	2
We 1-8	19 48 52.7	+22 25 15.5	19	19	R	as	T	A		59.30354	-1.72634	2
K 3-46	19 50 00.2	+33 45 51.2	36.2	23.5	B	prs	T	A		69.21381	3.80773	2
M 2-48	19 50 28.5	+25 54 30.2	19.4	11.3	B	mps	T	A		62.49376	-0.26996	2
PC 23	19 51 52.7	+32 59 17.9	5	2	R		T	A		68.74299	3.07667	2
K 3-48	19 52 09.1	+27 18 31.0			E		T	A		63.88897	0.12291	2
K 3-49	19 54 00.6	+33 22 12.5	3		R		T	A		69.29999	2.8887	2
K 4-41	19 56 34.0	+32 22 13.0	3	3	R		T	A		68.72031	1.91273	2
Abell 68	20 00 10.6	+21 42 56.0	38		B	as	T	A		60.04569	-4.33425	2
NeVe 2	20 00 18.7	+36 59 34.2	28		E	ms	T	A		73.07115	3.6667	2
K 3-52	20 03 11.4	+30 32 34.1	2.5	2.2	B	am	T	A		67.90799	-0.24943	2
K 3-53	20 03 22.4	+27 00 54.9	6		R	m	T	A		64.94128	-2.15956	2
ARO 342	20 04 16.1	+39 35 32.9	28	28	R	ars	T	A		75.69607	4.37686	2
M 1-75	20 04 44.1	+31 27 24.4	63	23	B	amrs	T	A		68.85755	-0.04165	2
K 3-54	20 04 58.6	+25 26 37.4			R		L	A		63.80104	-3.30052	2
NGC 6881	20 10 52.5	+37 24 42.7	16.8		B	amps	T	A		74.5523	2.11388	2
KjPn 1	20 12 24.0	+40 45 29.5	5.6	5.6	R	ams	T	A		77.51951	3.69643	2
K 3-57	20 12 47.7	+34 20 32.5	6.3	6.3	E	ms	T	A		72.19912	0.10436	2
Hen 2-459	20 13 57.9	+29 33 55.9	3	2	B	mrs	T	A		68.35072	-2.73822	2
KjPn 2	20 15 22.2	+40 34 44.8	3.5	3.5	B	a	L	A		77.68066	3.12777	2
NGC 6894	20 16 24.0	+30 33 53.2	56.4	53.3	E	mrs	T	A		69.47555	-2.62239	2

Table A1 *continued*

Table A1 (*continued*)

Name	R. A. (J2000) ($^{\text{h}}\text{m}^{\text{s}}$)	Decl. (J2000) ($^{\circ}\text{'}$ $''$)	D_{maj}	D_{min}	M. Mor.	S. Mor.	Class	Grade	Notes	l ($^{\circ}$)	b ($^{\circ}$)	Ref.
(1)	(2)	(3)	(4)	(5)	(6)	(7)	(8)	(9)	(10)	(11)	(12)	(13)
CLU PLANETARY NEBULAE												
KjPn 3	20 17 15.5	+38 50 23.9	3	3	S	L	A		76.43742	1.85746	2	
Abell 69	20 19 58.3	+38 24 02.8	23	21	B	amrs	T	A	76.37255	1.17222	2	
M 3-35	20 21 03.8	+32 29 24.2	4.6	4	E	mprs	T	A	71.62842	-2.36174	2	
K 3-58	20 21 58.3	+29 59 22.2	20	10	B	mrs	T	A	69.67674	-3.94075	2	
K 3-76	20 25 04.9	+33 34 50.7	4.3		E	r	T	A	73.00594	-2.42924	2	
K 4-53	20 42 16.3	+37 40 29.3	20		B	amps	T	A	78.3792	-2.7993	2	
K 4-55	20 45 10.0	+44 39 14.6	71	30	B	mrs	T	A	84.20035	1.09115	2	
K 3-78	20 45 22.7	+50 22 39.9	6	5	R	T	A		88.71361	4.61954	2	
NGC 7026	21 06 18.6	+47 51 06.7	39	18	B	amps	T	A	89.00201	0.37524	2	
K 3-80	21 07 39.7	+40 57 52.3	6	6	E	m	T	A	84.06671	-4.43944	2	
We 1-11	21 10 52.3	+50 47 14.8	27	24	B	prs	T	A	91.66514	1.81757	2	
NGC 7048	21 14 15.2	+46 17 17.5	63	60	E	mrs	T	A	88.78003	-1.68024	2	
K 3-60	21 27 26.5	+57 39 06.4	3	2	B	as	T	A	98.26472	4.90666	2	
K 3-61	21 30 00.7	+54 27 27.5	8	6	E	ars	T	A	96.31663	2.34698	2	
K 3-82	21 30 51.5	+50 00 08.5	24	21.5	E	prs	T	A	93.36129	-0.99007	2	
K 3-62	21 31 50.2	+52 33 51.6	5	3	S	T	A		95.22053	0.7793	2	
K 3-83	21 35 43.9	+50 54 17.0	6		B	mps	T	A	94.54317	-0.85136	2	
K 3-84	21 38 49.0	+46 00 27.8	8	8	E	mr	T	A	91.64882	-4.83735	2	
K 3-63	21 39 12.0	+55 46 03.9	7	7	B	mps	T	A	98.17165	2.42836	2	
M 2-49	21 43 17.6	+50 25 14.6	3	3	R	ms	T	A	95.1221	-2.00695	2	
M 2-50	21 57 41.8	+51 41 39.0	16	7	B	ars	T	Aborted		97.68216	-2.45171	2
Bl 2-1	22 20 16.6	+58 14 16.6	1.6	1.6	E	rs	T	A		104.11122	1.00115	2
M 2-52	22 20 30.7	+57 36 21.6	24		B	ams	T	A		103.79293	0.45432	2
M 2-53	22 32 17.7	+56 10 26.1	20	15	B	mprs	T	A		104.40729	-1.60995	2
NGC 7354	22 40 19.9	+61 17 08.7	33	31	B	mps	T	A		107.84362	2.31539	2
K 3-87	22 55 07.0	+56 42 31.1	6	6	R	T	A			107.44232	-2.62373	2
M 1-80	22 56 19.8	+57 09 20.7	8	8	R	as	T	A		107.78467	-2.29161	2
PM 1-339	22 58 51.6	+61 57 43.9	5.5		B	m	T	A		110.114	1.92495	2

Table A1 (*continued*)

Table A1 (*continued*)

Name	R. A. (J2000) (^h ^m ^s)	Decl. (J2000) (^o ['] ["])	D_{maj}	D_{min}	M. Mor.	S. Mor.	Class	Grade	Notes	l (^o)	b (^o)	Ref.
(1)	(2)	(3)	(4)	(5)	(6)	(7)	(8)	(9)	(10)	(11)	(12)	(13)
WeSb 6	23 13 04.0	+59 17 39.9	82	80	R	ars	T	A		110.65993	-1.21316	2
KjPn 8	23 24 10.5	+60 57 30.7	458.3	B	amps	L	A			112.53869	-0.14005	2
PM 1-20	06 28 04.1	+12 46 21.8	36	I	mp	T	B	Bright Neighbor; Clearer in Band 2	198.92438	0.7137	3	
CBSS 2	18 56 15.7	-01 34 00.3	4.9	3.6	E	p	T	A		32.08686	-1.78733	3
PM 1-273	19 01 05.8	+08 25 36.0		S		L	A		41.52932	1.70382	3	
PM 1-281	19 06 32.1	+10 43 23.9	R			T	A		44.18613	1.56318	3	
PM 1-286	19 11 35.8	+13 31 11.6		S		P	A		47.23947	1.75262	3	
PM 1-290	19 13 19.1	+15 39 39.7		S		L	A		49.33211	2.37274	3	
AGP 2	19 13 37.2	+10 39 32.9	42	B	amp	T	A		44.93256	-0.01042	3	
KLW 1	19 25 40.5	+16 33 05.0	12	E	mrs	T	A		51.5096	0.16774	3	
KLSS 1-2	19 26 40.1	+20 29 15.0		E	ar	T	A		55.08578	1.83036	3	
PM 1-309	19 37 29.3	+23 09 46.6		S		P	A		58.64103	0.9196	3	
KLW 4	19 49 58.8	+30 14 53.9	13.7	E	r	T	A		66.1756	2.03126	3	
TaWe 4	19 54 17.2	+35 07 03.4	13	E	mr	T	A		70.83173	3.7364	3	
KLSS 2-3	19 59 55.8	+34 29 04.8	22.8	E	prs	T	A		70.89168	2.41755	3	
KLW 5	20 00 42.0	+32 27 40.9		E	rs	T	A		69.2544	1.21687	3	
KLSS 2-6	22 30 06.8	+56 11 53.8	17	E	ar	T	Aborted	No CLU image	104.15883	-1.4338	3	
PM 1-264	18 54 54.1	+05 48 11.3	3	S		T	A		38.4924	1.87511	4	
PM 1-316	20 00 52.9	+34 28 22.2		S		P	A		70.98479	2.24447	4	
Ri 1	06 46 24.7	+08 29 02.0	70	62	E	ars	T	A		204.80576	2.74952	5
Te 6	19 09 54.7	+12 04 55.2	18	B		T	A		45.77374	1.45349	5	
Kn 15	19 40 40.3	+29 30 10.5	26.3	E	mrs	T	A		64.52054	3.40738	5	
Kn 7	19 42 26.0	+21 45 21.1	27.4	15.7	B		A		57.97967	-0.76789	5	
IPHASX J200457.3+311416	20 04 57.8	+31 14 17.5	26	B	m	P	A		68.69903	-0.19986	5	
Ri 2	20 50 02.8	+37 53 15.7	38	28	E	ars	T	A		79.50494	-3.8688	5
IPHASX J012507.9+635652	01 25 07.9	+63 56 52.8	22	12	B	apm	T	A		126.62168	1.3179	6
PHR J0650+0013	06 50 40.5	+00 13 40.1	40	25	B	mps	T	A		212.6422	-0.0659	7
PHR J1900-0014	19 00 03.3	-00 14 01.2	48	35	E	pr	T	A		33.70659	-2.02389	7

Table A1 *continued*

Table A1 (*continued*)

Name	R. A. (J2000) ($^{\text{h}}\text{m}^{\text{s}}$) (2)	Decl. (J2000) ($^{\circ}\text{'}\text{''}$) (3)	D_{maj} ($''$) (4)	D_{min} ($''$) (5)	M. Mor. (6)	S. Mor. (7)	Class (8)	Grade (9)	Notes (10)	l ($^{\circ}$) (11)	b ($^{\circ}$) (12)	Ref. (13)
CLU PLANETARY NEBULAE												
MPA J1841-0140	18 41 04.6	-01 40 49.6	10	8	E	as	T	A	30.2543	1.5378	8	
MPA J1842+0050	18 42 11.4	+00 50 31.8	6	6	R		T	A	32.6273	2.4416	8	
MPA J1852-0044	18 52 24.1	-00 44 46.4	5	5	R		T	A	32.3777	-0.5548	8	
MPA J1852-0033	18 52 25.5	-00 33 26.2	9	9	S		T	A	32.5485	-0.4738	8	
MPA J1852-0210	18 52 55.8	-02 10 56.5	8	7	E		T	A	31.1594	-1.3269	8	
MPA J1854-0139	18 54 48.2	-01 39 22.0	6	5	E		T	A	31.8413	-1.5038	8	
MPA J1855-0048	18 55 25.7	-00 48 22.8	11	10	E		T	A	32.6691	-1.2555	8	
MPA J1901+0000	19 01 36.0	+00 00 10.9	7	7	R		T	A	34.0937	-2.2596	8	
BMP J1917+0200	19 17 07.3	+02 00 10.1	76	64	E	a	T	B	Faint	37.6558	-4.7916	8
V458 Vul	19 54 24.6	+20 52 52.2	27	17	B	ps	T	A	58.63306	-3.61715	9	
PM 1-242	18 34 38.6	+00 08 04.0			E		T	A	31.13461	3.79733	10	
PM 1-318	20 09 32.8	+37 31 16.9	7	R	r		T	A	74.50065	2.39435	10	
GLMP 844	18 54 34.8	+00 11 04.6	3.5	S		T	A	33.4544	-0.61491	11		
GLMP 879	19 09 30.1	+09 02 25.4	2	S		L	B		43.02822	0.13993	11	
NVSS J192414+153909	19 24 14.6	+15 39 11.2	4	S		L	A		50.55558	0.04483	11	
IRAS 02379+5724	02 41 37.0	+57 37 44.5	7	E		P	A		137.2771	-2.14131	12	
IPHAS J053440.77+254238.2	05 34 39.8	+25 42 25.3	60	B		P	B		181.44833	-3.77509	12	
IPHAS J192717.94+081429.4	19 27 17.9	+08 14 29.4		P		A			50.04322	1.73943	12	
IPHASX J221118.0+552841	22 11 18.0	+55 28 41.9	35	29	B	as	T	A	44.37616	-4.1229	12	
IRAS 00032+6348	00 05 53.5	+64 05 15.6		P		A			101.55136	-0.60083	12	
[MCG2003] IC 10 PN 7	00 20 22.2	+59 20 01.7		P		A			117.98044	1.65467	13	
IPHASX J022045.0+631134	02 20 45.1	+63 11 34.9	30	0	B	as	T	A	138.5222	-0.08888	13	
IPHASX J025658.2+585547	02 56 58.2	+58 55 47.2	12	6	B		L	A	157.90114	-2.20974	13	
IRAS 04260+4513	04 29 39.2	+45 19 53.3		S		P	A		174.59446	-3.00814	13	
IPHAS J052015.87+314938.8	05 20 15.9	+31 49 38.8	40	E	ar	P	A		183.0219	0.01762	13	
IPHASX J055242.8+262116	05 52 42.8	+26 21 16.1	16.1	R	amr	T	A		210.83584	-2.74396	13	
IPHAS J063750.80+003644.0	06 37 50.8	+00 36 44.0		S		P	A					

Table A1 *continued*

Table A1 (*continued*)

Name	R. A. (J2000) ($^{\text{h}}\text{m}^{\text{s}}$) (1)	Decl. (J2000) ($^{\circ}\text{'}\text{''}$) (2)	D_{maj} ($''$) (3)	D_{min} ($''$) (4)	M. Mor. (5)	S. Mor. (6)	Class (7)	Grade (8)	Notes (9)	l ($^{\circ}$) (10)	b ($^{\circ}$) (11)	Ref. (13)
IPHASX J183249.6-005638	18 32 49.7	-00 56 38.3	4.6	5.6	S	T	A			29.96546	3.70772	13
IPHAS J183531.31-001550.0	18 35 31.3	-00 15 50.0			S	P	A			30.88007	3.4201	13
IRAS 18389-0030	18 41 25.9	-00 27 45.5			S	P	A			31.37885	2.01487	13
IPHAS J184139.13-021649.3	18 41 39.1	-02 16 49.3			S	P	B			29.78646	1.13544	13
IRAS 18390-0128	18 41 40.4	-01 25 17.7			E	T	A			30.55295	1.52319	13
IPHAS J184546.74+003630.9	18 45 46.7	+00 36 31.6	4		R	T	A			32.82865	1.53673	13
IPHAS J184616.33-030626.0	18 46 16.3	-03 06 25.6	3.8	3.8	S	m	L	A		29.57802	-0.26842	13
IPHAS J184853.00+012852.2	18 48 53.0	+01 28 52.2			S	T	A			33.95918	1.24361	13
IPHAS XJ185309.4+075241	18 53 09.4	+07 52 41.0	12.2	8.1	E	am	T	A		40.14563	3.20376	13
IPHAS J185321.76+055641.9	18 53 21.8	+05 56 41.9	5	5	R	T	A			38.44447	2.28061	13
IPHASX J185957.0+073544	18 59 57.0	+07 35 44.5	3.7	3.7	B	T	B			40.66018	1.57664	13
IPHAS J190414.21+115206.6	19 04 14.2	+11 52 06.6			S	P	A			44.94648	2.58872	13
IPHAS J190518.33+105750.5	19 05 18.3	+10 57 50.5	4		R	T	A			44.26153	1.942	13
IPHASX J190841.9+153332	19 08 41.8	+15 33 32.9			B	a	P	A		48.72888	3.31371	13
IRAS 19089+1032	19 11 17.2	+10 37 34.2	4.2	4.2	S	L	A			44.63764	0.48268	13
IPHAS J191508.90+150951.5	19 15 08.9	+15 09 51.5			S	T	A			49.0961	1.75179	13
IPHAS J191621.43+165638.9	19 16 21.4	+16 56 38.9	5.3	5.3	R	T	A			50.80823	2.32144	13
IPHASX J191727.0+082036	19 17 27.0	+08 20 37.0	15.2	15.2	R	as	T	A		43.32176	-1.92348	13
IPHASX J191727.2+142735	19 17 27.3	+14 27 35.0			S	L	A			48.73195	0.93046	13
IPHAS J191907.59+094849.8	19 19 07.6	+09 48 49.8			S	P	A			44.81574	-1.60282	13
IRAS 19171+1536	19 19 22.9	+15 41 37.2			R	T	A			50.04051	1.09601	13
IRAS 19174+1615	19 19 42.9	+16 21 28.0	4	4	E	T	A			50.66485	1.33646	13
IPHAS J192009.35+230816.6	19 20 09.4	+23 08 16.6			B	T	A			56.71752	4.41012	13
IRAS 19183+1727	19 20 31.6	+17 32 49.1			S	P	A			51.80671	1.72239	13
IPHAS J192054.53+174607.9	19 20 54.5	+17 46 07.9			E	L	A			52.04545	1.74615	13
IPHAS J192101.15+103734.6	19 21 01.1	+10 37 34.6	3		E	L	A			45.75205	-1.63346	13
IPHAS J192348.79+052759.9	19 23 48.8	+05 27 59.9			E	T	A			41.51175	-4.66302	13
IPHAS J192553.53+165331.4	19 25 53.5	+16 53 31.4	5.7	4.9	E	T	A			51.83409	0.28379	13

Table A1 *continued*

Table A1 (*continued*)

Name	R. A. (J2000) ($^{\text{h}}\text{m}^{\text{s}}$) (1)	Decl. (J2000) ($^{\circ}\text{'}\text{''}$) (2)	D_{maj} ($''$) (3)	D_{min} ($''$) (4)	M. Mor. ($''$) (5)	S. Mor. ($''$) (6)	Class (7)	Grade (8)	Notes (9)	l ($^{\circ}$) (10)	b ($^{\circ}$) (11)	Ref. (13)
IPHAS J192847.9+211922	19 28 47.9	+21 19 22.8	S	L	A					56.0578	1.79095	13
IPHAS X J192902.5+244646	19 29 02.5	+24 46 46.8	9.9	8.7	R	ms	T	A		59.1263	3.38966	13
IPHAS X J193532.1+112115	19 35 32.1	+11 21 15.7	9.2	9.2	R		T	A		48.0909	-4.421	13
IPHAS X J193652.96+171940.7	19 36 53.0	+17 19 40.7	4.1	4.1	R		T	A		53.48033	-1.80822	13
IPHAS X J193740.4+203547	19 37 40.5	+20 35 47.8	30.7	30.7	I	as	T	A		56.42408	-0.374	13
IPHAS X J193949.8+264047	19 39 49.8	+26 40 47.4	B	mp	P		P	A		61.96748	2.18184	13
2MASS J19453289+2328105	19 45 32.9	+23 28 10.5	2.5	E		L	T	A		59.82359	-0.53609	13
IPHAS X J194648.2+193608	19 46 48.4	+19 36 11.1	3	B	p	T	T	A		56.62379	-2.72839	13
IPHAS J194727.51+241502.1	19 47 27.5	+24 15 02.1	S	P	P		P	A		60.71833	-0.52103	13
IRAS 19461+2419	19 48 14.3	+24 27 27.0	S	T	T		T	A		60.98662	-0.56988	13
IPHAS J194957.59+232600.6	19 49 57.6	+23 26 00.6	3.5	S	T		T	A		60.30303	-1.42787	13
IPHAS J195116.18+205954.2	19 51 16.2	+20 59 54.2	S	P	P		P	A		58.35873	-2.92687	13
IPHAS X J195126.5+265839	19 51 26.5	+26 58 39.0	7.7	6.8	B	T	T	A		63.52364	0.08932	13
IPHAS J195224.67+230856.2	19 52 24.7	+23 08 56.2	S	P	P		P	A		60.34517	-2.05718	13
IPHAS X J195248.8+255559	19 52 48.8	+25 53 59.2	27	B	L		L	A		62.75515	-0.72631	13
IPHAS J195323.06+235533.4	19 53 23.1	+23 55 33.4	S	P	P		P	A		61.12714	-1.85048	13
IPHAS J195509.17+315416.6	19 55 09.2	+31 54 16.6	S	P	P		P	A		68.1666	1.92779	13
IPHAS X J195549.80+311340.0	19 55 49.8	+31 13 40.0	S	P	P		P	A		67.66173	1.45425	13
IPHAS J195912.66+335003.9	19 59 12.7	+33 50 03.9	S	P	P		P	A		70.25941	2.20346	13
IPHAS X J195919.0+312534	19 59 19.1	+31 25 34.3	7.6	5.3	E	L	A			68.21947	0.92205	13
IRAS 19581+3320	20 00 06.9	+33 29 01.0	P	A						70.05928	1.8593	13
2MASS J20011443+3331220	20 01 14.4	+33 31 22.2	P	A						70.21625	1.6805	13
IPHAS J200522.65+393858.3	20 05 22.6	+39 38 58.3	90	R	s	P	P	A		75.85836	4.22624	13
IPHAS J201714.26+353927.4	20 17 14.3	+35 39 27.4	S	P	P		B			73.79818	0.0786	13
IPHAS J201954.23+430559.6	20 19 54.2	+43 05 59.6	R	T	T		A			80.24768	3.83617	13
IPHAS J203346.47+450840.1	20 33 46.5	+45 08 40.1	S	T	T		A			83.36094	2.99023	13
IPHAS X J212608.3+542015	21 26 08.4	+54 20 15.4	13	8.5	B	as	T	A		95.82574	2.64949	13
IPHAS X J214032.5+564751	21 40 32.6	+56 47 51.6	9.4	9.4	R	r	T	A		98.99328	3.07793	13

Table A1 *continued*

Table A1 (*continued*)

Name	R. A. (J2000) ($^{\text{h}}\text{m}^{\text{s}}$)	Decl. (J2000) ($^{\circ}\text{'}$ $''$)	D_{maj}	D_{min}	M. Mor.	S. Mor.	Class	Grade	Notes	l ($^{\circ}$)	b ($^{\circ}$)	Ref.
(1)	(2)	(3)	(4)	(5)	(6)	(7)	(8)	(9)	(10)	(11)	(12)	(13)
IPHAS J215919.15+594009.9	21 59 19.2	+59 40 09.9			P	B	Faint; Close to HASH Images		102.73037	3.72889	13	
Te 10	00 13 33.8	+67 18 04.0	13	7	B		T	A	119.28001	4.69828	14	
Te 5	04 03 29.5	+52 08 26.0	24.9	18	B	p	T	A	150.07352	-0.30836	14	
HoCr 1	06 21 41.0	+23 35 12.8	73	59	B	amps	T	A	188.63669	4.40816	14	
Pa 6	20 09 41.0	+41 14 42.8	46.3		R	ars	T	A	77.64943	4.39152	14	
Te 8	20 55 27.3	+39 03 59.2	23	18	B		T	A	81.09144	-3.93151	14	
Pa 7	21 20 00.1	+51 41 05.7	9	6	B	ps	T	A	93.30349	1.4107	14	
Kn 28	21 22 01.0	+55 04 30.0	56	34	B	ams	T	A	95.91781	3.55288	14	
Te 4	23 27 13.2	+65 09 23.0	19	17	R	s	T	A	114.23215	3.71695	14	
IPHASX J194359.5+170901	19 43 59.5	+17 09 01.1	21		B	amps	T	A	54.16148	-3.37347	15	
IPHASX J052531.1+281945	05 25 31.2	+28 19 46.4	10.1		E	s	T	A	178.13108	-4.04106	16	
Ou 1	04 07 21.6	+51 24 22.4	95	75	I	L	A		151.009	-0.45698	17	
Ou 3	19 38 17.5	+23 45 48.7	90	90	R	ar	T	C	59.25498	1.05307	17	
Pa 19	19 05 08.6	+16 15 20.6	35	32	E	ar	L	C	48.95976	4.3917	18	
Pa 24	20 11 44.4	+24 50 06.0	42	39	E	rs	T	B	64.11347	-4.91781	18	
IPHASX J000021.4+572207	00 00 21.0	+57 22 07.7	22	16	B		L	B				
IPHASX J005123.2+631059	00 51 23.2	+63 10 59.1	47	30.9	A		P	B				
IPHASX J013108.9+612258	01 31 09.0	+61 22 59.0	24.1	24.1	R	a	T	B				
IPHASX J015624.9+652830	01 56 24.9	+65 28 30.4	212	198	R	ar	T	A				
IPHASX J023538.6+633823	02 35 39.4	+63 38 23.9	134.5	134.5	E	a	T	Aborted				
IPHASX J030421.3+621802	03 04 21.3	+62 18 02.5	57	0	R	r	T	A				
IPHASX J031345.5+613707	03 13 45.1	+61 37 06.0	126.5	104.4	E	s	T	B				
IRAS 03272+5528	03 31 05.4	+55 38 51.4	27.3	25.7	E	ar	T	A				
IPHASX J034659.8+484900	03 46 59.8	+48 49 00.2	62		R	a	P	B				
IPHASX J043826.1+483907	04 38 26.2	+48 39 07.8	95		E	as	P	A				
IPHASX J045358.6+465842	04 53 58.7	+46 58 42.7	24		A	m	P	A				
IPHASX J045627.6+501720	04 56 27.6	+50 17 20.4	91		R	a	T	A				
IPHASX J045847.7+373640	04 58 47.7	+37 36 40.8	16.9	16.9	R	a	T	A				

Table A1 *continued*

Table A1 (*continued*)

Name	R. A. (J2000) ($^{\text{h}}\text{m}^{\text{s}}$)	Decl. (J2000) ($^{\circ}\text{'}\text{''}$)	D_{maj}	D_{min}	M. Mor.	S. Mor.	Class	Grade	Notes	l ($^{\circ}$)	b ($^{\circ}$)	Ref.	
(1)	(2)	(3)	(4)	(5)	(6)	(7)	(8)	(9)	(10)	(11)	(12)	(13)	
IPHASX J051733.3+393027	05 17 33.3	+39 30 27.5	65	A	P	A			167.98842	0.95153	19		
IPHASX J060328.1+154108	06 03 28.1	+15 41 08.5	55	E	a	T	B	Faint; Resolved in One Epoch	193.52156	-3.13879	19		
IPHASX J060412.2+190031	06 04 12.2	+19 00 31.5	70	0	B	a	T	Faint	190.70904	-1.35667	19		
IPHASX J060416.2+133250	06 04 16.3	+13 32 50.4	34.6	10.6	B	a	L	A	195.48612	-4.01397	19		
IPHASX J062937.8+065220	06 29 37.9	+06 52 20.1	31	B	a	T	A		204.3301	-1.68385	19		
IPHASX J063223.9+150410	06 32 23.9	+15 04 10.3	90	B	T	B	Faint		197.37333	2.70781	19		
IPHASX J184030.1-003822	18 40 30.1	-00 38 22.2	22.2	22.2	B		L	C	Small; Faint	31.11507	2.14111	19	
IPHASX J184834.6+063302	18 48 34.7	+06 33 02.7	21	B	a	T	A		38.44485	3.61516	19		
IPHASX J185225.0+080843	18 52 25.0	+08 08 43.8	22.4	22.4	R		T	D	40.30129	3.48826	19		
IPHASX J185225.8+005250	18 52 25.8	+00 52 50.0	480	E	ars	P	C		33.82874	0.18074	19		
IPHASX J185312.9-002529	18 53 12.9	-00 25 30.0	25.8	17	E		L	C	32.75632	-0.58928	19		
IPHASX J185342.6-003628	18 53 42.6	-00 36 28.8	22.8	22.8	E		L	B	32.64978	-0.78275	19		
IPHASX J185640.0-003804	18 56 40.0	-00 38 04.5	15	B	p	T	A		32.96318	-1.45279	19		
IPHASX J185744.4+105053	18 57 44.4	+10 50 53.2	109.5	E	ams	T	B	Partially Resolved	43.31089	3.54235	19		
IPHASX J185815.8+073753	18 58 15.9	+07 37 53.5	7.1	6.3	R	T	A		40.50141	1.96481	19		
IPHASX J190115.5+114150	19 01 15.5	+11 41 50.7	25.8	25.8	E	ar	T	B	44.4613	3.15942	19		
IPHASX J190227.3+020804	19 02 27.3	+02 08 04.7	92	I	as	T	C	Irregular HII region	36.00849	-1.47568	19		
IPHASX J190319.0+142524	19 03 19.0	+14 25 24.5	14.6	12	E	T	B	Faint	47.12242	3.95213	19		
IPHASX J190340.4+045311	19 03 40.4	+04 53 11.5	113.8	49.9	I		P	C	Dense Bright Neighbors	38.67447	-0.48569	19	
IPHASX J190340.7+094639	19 03 40.8	+09 46 39.2	19.6	14	E	m	T	A		43.02299	1.75424	19	
IPHASX J190417.9+084916	19 04 17.9	+08 49 16.3	4.5	4.5	S	T	A		42.24254	1.18042	19		
IPHASX J190432.9+091656	19 04 32.9	+09 16 56.7	8.2	8.2	E		T	A	42.68093	1.33682	19		
IPHASX J190447.9+121844	19 04 48.0	+12 18 44.7	12.2	9.2	E	r	T	A	45.40471	2.66915	19		
IPHASX J190454.0+101801	19 04 54.1	+10 18 01.0	18.2	16.3	E	ars	T	A		43.62569	1.72622	19	
IPHASX J190503.1+034225	19 05 03.2	+03 42 25.6	64	E	ar	T	C	Dense Bright Neighbors	37.78389	-1.33206	19		
IPHASX J190512.4+161347	19 05 12.5	+16 13 47.4	63	58	R	ar	T	A	48.94364	4.36623	19		
IPHASX J190543.8+110018	19 05 43.8	+11 00 18.5	7.6	7.6	R	r	T	A	44.34595	1.86811	19		
IPHASX J190631.5-023236	19 06 31.6	-02 32 36.0	16.1	16.1	E		L	C	Too Faint	32.38452	-4.51544	19	

Table A1 *continued*

Table A1 (*continued*)

Name	R. A. (J2000) ($^{\text{h}}\text{m}^{\text{s}}$)	Decl. (J2000) ($^{\circ}\text{'}$ $''$)	D_{maj}	D_{min}	M. Mor.	S. Mor.	Class	Grade	Notes	l ($^{\circ}$)	b ($^{\circ}$)	Ref.
(1)	(2)	(3)	(4)	(5)	(6)	(7)	(8)	(9)	(10)	(11)	(12)	(13)
IPHASX J190718.1+044056	19 07 18.1	+04 40 56.1	9.3	3.3	B	T	B	Band 2 Brighter Than 1	38.90802	-1.3827	19	
IPHASX J191001.1+142202	19 10 01.1	+14 22 02.7	9.7	9.7	E	T	A		47.81546	2.48313	19	
IPHASX J191022.1+110538	19 10 22.1	+11 05 38.5	9.7	9.7	E	ar	T	A	44.94852	0.89862	19	
IPHASX J191027.4+034046	19 10 27.4	+03 40 46.9	13.3	13.3	R	a	T	A	38.37923	-2.54221	19	
IPHASX J191255.4+143248	19 12 55.5	+14 32 48.1	7.5	7.5	R	ar	T	A	48.29939	1.94168	19	
IPHAS XJ191345.6+174752	19 13 45.6	+17 47 52.3	6.5	6.5	R	as	T	A	51.27847	3.26611	19	
IPHASX J191445.1+133219	19 14 45.1	+13 32 19.9	15.4	11.5	E	ars	T	A	47.61158	1.08181	19	
IPHASX J191651.6+065608	19 16 51.6	+06 56 08.6	17.3	7.9	A	L	C		42.00665	-2.4494	19	
IPHASX J191716.4+033447	19 17 16.4	+03 34 47.4	32	32	E	mr	T	B	39.07646	-4.09718	19	
IPHASX J191716.5+181518	19 17 16.6	+18 15 18.2	46.1	46.1	R	rs	T	A	52.07192	2.73693	19	
IPHASX J191840.4+073131	19 18 40.4	+07 31 31.1	41.2	41.2	E	a	T	C	42.73856	-2.57289	19	DU ET AL.
IPHASX J192146.7+172055	19 21 46.7	+17 20 55.9	29	E	ars	T	A		51.772	1.36581	19	
IPHASX J192152.0+135223	19 21 52.0	+13 52 23.2	13	B		T	A		48.71534	-0.28937	19	
IPHASX J192153.9+143056	19 21 53.9	+14 30 56.2	18.3	13.6	E	ar	T	A	49.28575	0.00645	19	
IPHASX J192436.3+154402	19 24 36.3	+15 44 02.0	22.6	14.6	E	a	T	A	50.66809	0.00612	19	
IPHASX J192534.9+200334	19 25 35.0	+20 03 34.1	38	E		L	B		54.58789	1.85149	19	
IPHASX J192543.2+143546	19 25 43.2	+14 35 46.3	176	R	ars	L	B		49.794	-0.77021	19	
IPHASX J192837.7+245024	19 28 37.8	+24 50 24.8	12.7	9.2	E	as	T	A	59.13502	3.50093	19	
Fe 1	19 28 47.3	+09 34 38.1	68.2	57.7	B	r	T	A	45.73016	-3.8145	19	
IPHASX J193009.3+192129	19 30 09.3	+19 21 29.0	221	E	ars	T	A		54.48448	0.57117	19	
UWISH2 PN 4	19 31 10.8	+19 29 05.7	19	B	a	T	A		54.7118	0.42027	19	
IPHASX J193127.0+115622	19 31 27.0	+11 56 22.9	26.7	26.7	R	T	B	Faint	48.12298	-3.26259	19	
IPHASX J193308.9+155354	19 33 08.9	+15 53 54.6	27	E	ars	T	B	Faint	51.79555	-1.71973	19	
IPHASX J193517.8+223120	19 35 17.8	+22 31 20.5	21	R	as	P	B	Faint	57.83543	1.04805	19	
IPHASX J193630.2+312810	19 36 30.3	+31 28 10.6	404	A	a	P	Aborted	Unusable CLU Image	65.80568	5.14851	19	
IPHASX J193633.5+153345	19 36 33.5	+15 33 45.3	103	R	T	B		Dense Bright Neighbors	51.89951	-2.60031	19	
IPHASX J193718.6+202102	19 37 18.7	+20 21 03.0	47	B	as	T	A		56.1681	-0.42008	19	
IPHASX J193752.2+271119	19 37 52.3	+27 11 19.8	25	E	T	B		Faint; Bright Neighbor	62.19767	2.81172	19	

Table A1 (*continued*)

Table A1 (*continued*)

Name	R. A. (J2000) (^h ^m ^s)	Decl. (J2000) ([◦] [′] [″])	D_{maj}	D_{min}	M. Mor.	S. Mor.	Class	Grade	Notes	l ([◦])	b ([◦])	Ref.
(1)	(2)	(3)	(4)	(5)	(6)	(7)	(8)	(9)	(10)	(11)	(12)	(13)
IPHASX J193827.8+265752	19 38 27.9	+26 57 52.1	6.4	6.4	R	r	T	Aborted	Unusable CLU Image	62.06633	2.5868	19
IPHASX J194232.8+150034	19 42 32.9	+15 00 34.2	18.6	18.6	R	ar	T	A	Dense Bright Neighbors	52.12485	-4.13062	19
IPHASX J194240.5+275109	19 42 40.6	+27 51 09.0	74	74			T	A		63.30053	2.21058	19
IPHASX J194510.6+270930	19 45 10.7	+27 09 30.0	14.3	9.7	B		L	A		62.97465	1.38387	19
IPHASX J194533.6+210808	19 45 33.6	+21 08 08.6	68.5	A	as		T	A		57.8047	-1.70772	19
IPHASX J194556.2+232833	19 45 56.2	+23 28 33.6	53.6	29.3	B	as	P	B	Flat Continuum	59.8739	-0.61006	19
IPHASX J194633.0+231659	19 46 33.0	+23 16 59.6	12.5	12.5	E	a	T	A		59.7778	-0.82848	19
IPHASX J194727.5+230816	19 47 27.6	+23 08 16.6	34.5	34.5	R	ars	T	A		59.7548	-1.08223	19
Ra 17	19 47 28.9	+22 28 23.8	27	R	as	T	B	Faint		59.18574	-1.42144	19
IPHASX J194751.9+311818	19 47 51.9	+31 18 18.1	12.9	6.8	B		T	A		66.85869	2.95718	19
IPHASX J194905.2+181503	19 49 05.2	+18 15 03.6	33	A		P	B	Faint		55.72448	-3.87424	19
IPHASX J194930.9+273028	19 49 31.0	+27 30 28.3	84	R		T	B	Faint; Dense Star Field		63.76218	0.72771	19
IPHASX J194940.9+261521	19 49 40.9	+26 15 21.2	22.1	10.3	B	ps	T	A		62.70235	0.06016	19
IPHASX J195221.6+315859	19 52 21.7	+31 58 59.8	42	E	ar	T	C	TooFaint; Dense Bright Neighbors		67.9297	2.47622	19
IPHASX J195343.7+202635	19 53 43.7	+20 26 35.8	30.6	24.6	B		T	B	Faint	58.17442	-3.70465	19
MVP 1	19 53 58.2	+31 21 20.3	228	176	E	as	T	A		67.5661	1.86052	19
IPHASX J195400.8+315554	19 54 00.9	+31 55 54.8	30.3	30.3	R	ar	T	A		68.06546	2.14878	19
IPHASX J195436.4+313326	19 54 36.4	+31 33 26.4	12	10	E	mr	T	A		67.8091	1.84791	19
IPHASX J195657.6+265713	19 56 57.6	+26 57 13.4	28.7	24.8	B	ars	T	A		64.13724	-0.97649	19
IPHASX J195836.4+292314	19 58 36.5	+29 23 14.7	17.4	11.1	E	a	T	B	Faint	66.40279	-0.01604	19
IPHASX J200041.5+283023	20 00 41.6	+28 30 23.3	31	31	R	a	T	B	Faint; Bright Neighbor	65.89281	-0.86695	19
Ou 6	20 03 53.6	+35 22 50.2	14.9	12.4	B	ar	T	A		68.0469	0.03702	19
IPHASX J200522.0+36594	20 05 22.1	+36 59 42.8	10.5	8.4	E	as	T	A		72.08243	2.20168	19
IPHASX J200937.3+242903	20 09 37.3	+24 29 03.4	24	B	a	T	A			63.55599	-4.70374	19
IPHASX J201339.0+331507	20 13 39.0	+33 15 07.1	8.6	8	B		T	A		71.38789	-0.64564	19
IPHASX J202946.0+354926	20 29 46.1	+35 49 26.4	16.1	16.1	R	r	T	A		75.3928	-1.90881	19
IPHASX J204414.1+360737	20 44 14.2	+36 07 37.2	19	E	s	T	A			77.40045	-4.06301	19

Table A1 (*continued*)

Table A1 (*continued*)

Name	R. A. (J2000) ($^{\text{h}}\text{m}^{\text{s}}$) (1)	Decl. (J2000) ($^{\circ}\text{'}$ (2))	D_{maj} ($''$) (3)	D_{min} ($''$) (4)	M. Mor. (5)	S. Mor. (6)	Class (7)	Grade (8)	Notes (9)	l ($^{\circ}$) (10)	b ($^{\circ}$) (11)	Ref. (13)	
IPHASX J205013.6+465515	20 50 13.7	+46 55 15.2	77	62	B	ms	T	A		86.51913	1.82833	19	
IPHASX J212151.8+473301	21 21 51.9	+47 33 01.6	29.9	22.1	B	s	T	A		90.59183	-1.72514	19	
IPHASX J212335.3+484717	21 23 35.3	+48 47 17.8	18.8	13.7	B		T	A		91.66699	-1.04723	19	
IPHASX J215842.3+533003	21 58 42.3	+53 30 03.4	30.5	30.5	R	ar	T	A		98.90755	-1.11463	19	
IPHASX J231546.1+605551	23 15 46.2	+60 55 51.4	60	E	r	P	C			111.57164	0.18697	19	
IPHASX J233841.2+614146	23 38 41.2	+61 41 46.1	61.4	45.7	E	ars	T	A	Too Faint		114.42106	0.03242	19
IPHASX J234025.5+652147	23 40 25.6	+65 21 47.6	62	R	a	P	B		Faint; Bright Neighbor		115.61566	3.50512	19
IPHASX J234318.0+635717	23 43 18.1	+63 57 17.1	36	R		T	B		Faint		115.53691	2.06561	19
IPHASX J234403.8+603242	23 44 03.8	+60 32 42.4	22.1	R	as	T	B		Flat Continuum		114.7382	-1.25036	19
IPHASX J235044.2+640311	23 50 44.3	+64 03 11.8	26.3	24.2	B	a	L	B			116.35134	1.95979	19
IPHASX J235114.7+601026	23 51 14.8	+60 10 26.4	48	R	a	P	B				115.50882	-1.82739	19
Pa 32	03 11 05.3	+63 50 15.0	73	60	E	ar	P	B	Too Faint; Bad CLU Images		137.606	5.01858	20
Pa 35	18 56 55.4	-01 03 51.0	8.5	R		ar	T	A	Faint; Resolved in Band 2		32.60988	-1.70563	20
Pa 125	19 08 52.4	+12 02 41.3	3	S		T	A				45.62356	1.661199	20
Pa 132	19 23 11.5	+12 28 38.5	3.6	E		T	C				47.63637	-1.23179	20
Ra 54	06 14 40.0	+18 49 15.0	35	A	a	L	A				192.07112	0.71764	21
Pre 7	19 50 33.6	+30 15 21.7	36	36	B	a	T	A			66.24588	1.92743	21
Ou 7	19 52 45.4	+32 25 36.0	342	E	r	T	C				68.35392	2.63105	21
Ou 5	21 14 20.0	+43 41 36.0	33	20	B	mp	T	A	Too Faint; Dense Star Field				
IPHASX J055226.2+323724	05 52 26.2	+32 37 24.8	445	290	B	as	T	C	Too Faint; Clearer in Band 2				
FBP8	19 04 57.4	+07 44 15.2	4	E		T	B		Faint		41.35409	0.53887	23
FBP10	19 23 07.2	+16 59 22.9	2		L		B		Faint		51.60615	0.91396	23
FBP11	19 48 23.3	+26 49 26.8			T		B		Close to HASH Images		63.04548	0.59769	23
Pa J1843.0+0334	18 43 03.7	+03 34 29.0	10	10	P		B				35.16324	3.49077	24
Pa J1906.9+0413	19 06 59.7	+04 13 48.9	15	25		L	D		Faint; Unknown Morphology		38.47121	-1.52233	24
Pa J1915.6+1708	19 15 40.2	+17 08 04.6	60	45	B	P	C		Too Faint		50.90075	2.55534	24
Pa J1916.3+0702	19 16 23.6	+07 02 23.9	10	10	P	A					42.04504	-2.29815	24
Pa J2141.2+5146	21 41 14.7	+51 45 59.1	15	15	P	A					95.75929	-0.77865	24

Table A1 (*continued*)

Table A1 (*continued*)

Name	R. A. (J2000) ($^{\text{h}}\text{m}^{\text{s}}$)	Decl. (J2000) ($^{\circ}\text{'}\text{''}$)	D_{maj}	D_{min}	M. Mor.	S. Mor.	Class	Grade	Notes	l ($^{\circ}$)	b ($^{\circ}$)	Ref.	
(1)	(2)	(3)	(4)	(5)	(6)	(7)	(8)	(9)	(10)	(11)	(12)	(13)	
MoM Ji 1	01 16 44.7	+60 00 52.7	300	E	as	L	C		Too Faint	126.09251	-2.70172	25	
StDr 46	02 15 34.6	+60 11 00.9	66	B		T	A			133.21417	-0.99766	25	
LBN 157.08-03.61	04 20 43.8	+44 56 28.2	73	B	ms	P	A			157.0805	-3.60861	25	
Kn 131	04 50 17.7	+41 54 53.2	266	192	as	T	B	Faint; Only Seen Central Parts		162.93716	-1.6839	25	
StDr 162	05 11 02.0	+45 02 24.6	342		P	C		Too Faint; Unknown Morphology		162.78933	3.20302	25	
Dr 32	05 34 06.7	+39 56 03.2	60	60	R	a	T	A		169.41482	3.82977	25	
StDr 13	06 34 22.6	+07 22 20.2	450	R	as	T	A			204.43042	-0.40867	25	
Sot 1	18 52 16.7	-00 43 39.2	12		P	C				32.38023	-0.51884	25	
Ra 73	19 01 31.9	+01 20 41.1	6	B		L	B	Too Faint		35.28027	-1.63173	25	
Cop 5	19 11 25.4	+05 31 13.7	6		L	B		Faint		40.12522	-1.90761	25	
StDr 28	19 17 25.1	+20 52 31.2	120	B	as	T	B			54.41259	3.92308	25	
StDr 16	19 18 50.6	+03 27 20.6	144	A	s	P	B	Faint		39.14791	-4.5018	25	
StDr 85	19 29 50.3	+19 34 20.4	72	B	mr	P	B	Faint		54.63679	0.73934	25	
StDr 165	19 46 20.6	+34 23 38.4	48	R	a	L	C	Resolved Only in One Exposure		69.37938	4.7791	25	
RaEMol 1	19 47 52.6	+26 54 23.4	6	R	a	T	A			63.05902	0.73763	25	
Ra Objet 2	19 50 57.1	+33 47 33.8	18	R		T	A			69.33845	3.65211	25	
StDr 164	20 01 13.7	+25 19 34.9	186	E	as	L	C			63.25198	-2.6447	25	
StDr Objet 2	20 33 31.1	+44 08 45.4	36	R		P	A			82.53032	2.43279	25	
Alba-1	21 35 07.9	+52 11 32.4	33	17	B	mr	T	A		95.33897	0.16522	25	
StDr 43	22 16 18.2	+54 18 42.1	420	A	s	P	C			101.48553	-1.96978	25	
StDr 53	22 44 54.7	+55 09 25.6	18	R		L	B	Resolved Only in One Exposure		105.46507	-3.36514	25	
StDr 97	23 14 18.8	+55 59 33.9	50	E	a	P	C	Faint		109.59639	-4.34374	25	
IPHASX J051152.2+302751	05 11 52.2	+30 27 51.2	375	245	E	r	P			174.66947	-5.26164	26	
IPHASX J053650.8+245616	05 36 50.8	+24 56 16.7	300	225	B		L	C	Faint		182.36399	-3.77166	26
IPHASX J054310.5+223111	05 43 10.5	+22 31 11.2	24	E		P	B		Faint		185.1884	-3.82007	26
IPHASX J055711.7+282322	05 57 11.7	+28 23 22.4	224	E	as	T	A			181.76714	1.90378	26	
IPHASX J061602.5+175920	06 16 02.6	+17 59 20.6	274		P	D				192.95798	0.60803	26	
IPHASX J184836.2+022050	18 48 36.2	+02 20 50.7		S	P	A				34.69881	1.7003	26	

Table A1 *continued*

Table A1 (*continued*)

Name	R. A. (J2000) ($^{\text{h}}\text{m}^{\text{s}}$) (2)	Decl. (J2000) ($^{\circ}\text{'}$ (3))	D_{maj} ($''$) (4)	D_{min} ($''$) (5)	M. Mor.	S. Mor.	Class	Grade	Notes	l ($^{\circ}$) (10) (11)	b ($^{\circ}$) (12) (13)	Ref.
IPHASX J185322.1+083018	18 53 22.1	+08 30 18.0	110	R	ar	T	C		Too Faint	40.72916	3.44128	26
IPHASX J190333	19 03 36.6	+10 43 03.7	460	A		P	C		Too Faint; Dense Star Field	43.85173	2.19939	26
IPHASX J190419.4+152126	19 04 19.4	+15 21 26.6	470			P	C		Too Faint	48.0673	4.15959	26
IPHASX J190543.8+064413	19 05 43.8	+06 44 13.3	14	E	a	T	B		Too Faint	40.55342	-0.09107	26
IPHASX J191003.4+032224	19 10 03.4	+03 22 24.1	225	R	as	T	C		Too Faint	38.06096	-2.59444	26
IPHASX J191058.9+040350	19 10 58.9	+04 03 50.4	11	B	a	T	A		Only Resolved in Band 2	38.78112	-2.48159	26
IRAS 19086+0603	19 11 04.8	+06 08 45.1	32	22	B	am	T	A		40.64062	-1.54284	26
IPHASX J191421.0+140936	19 14 21.1	+14 09 36.3	42	R	ar	P	A			48.11677	1.45635	26
IRAS 19227+1928	19 24 58.2	+19 34 34.9	29	R		P	A			54.09396	1.7495	26
IPHASX J192510.5+113400	19 25 10.8	+11 33 53.6	100			P	A		Unknown Morphology	47.06172	-2.09148	26
IPHASX J193305.9+132921	19 33 05.9	+13 29 21.1	60	E	prs	T	A			49.67735	-2.87108	26
IPHASX J193617.5+272051	19 36 17.6	+27 20 51.9	9	R	a	T	A			62.16582	3.19535	26
IPHASX J193636.3+123758	19 36 36.5	+12 38 02.3	270	R	ar	L	B		Faint	49.34073	-4.03273	26
IPHASX J193809.1+205412	19 38 09.2	+20 54 12.1	146	E	a	L	C		Too Faint	56.74625	-0.32116	26
IPHASX J193849.6+313744	19 38 49.7	+31 37 44.8	160	E	ar	T	B		Too Faint	66.18609	4.79252	26
IPHASX J194301.3+215424	19 43 01.3	+21 54 24.9	14	B		T	B		Faint	58.17861	-0.81133	26
IPHASX J194645.3+262211	19 46 45.3	+26 22 11.5	290	A		P	C		Faint; Dense Star Field	62.46911	0.68376	26
IPHASX J194745.5+270150	19 47 45.5	+27 01 50.7	207	E	a	P	D		Too Faint; Bad CLU Images	63.15292	0.8232	26
IPHASX J195328.9+370957	19 53 28.9	+37 09 57.6	482.9	482.9		as	L	C	Faint	72.51438	4.92261	26
IPHASX J195627.3+250648	19 56 27.3	+25 06 48.6	24	E		L	C		Faint	62.50555	-1.83587	26
IRAS 20084+3604	20 10 17.9	+36 13 09.7	13.9	E	am	P	A			73.48972	1.55946	26
IPHASX J201058.0+284455	20 10 58.0	+28 44 55.0	48	36	B	ap	T	B	Faint	67.30744	-2.63959	26
IPHASX J225453.2+631827	22 54 53.2	+63 18 27.6	24	E		P	B		Faint; Bright Neighbor	110.27625	3.33648	26

Table A1 *continued*

Table A1 (*continued*)

Name (1)	R. A. (J2000) ($^{\text{h}}\text{ m} \text{s}$) (2)	Decl. (J2000) ($^{\circ} \text{ '} \text{ ''}$) (3)	D_{maj} ($''$) (4)	D_{min} ($''$) (5)	M. Mor. (6)	S. Mor. (7)	Class (8)	Grade (9)	Notes (10)	l ($^{\circ}$) (11)	b ($^{\circ}$) (12)	Ref. (13)
-------------	---	---	-------------------------------------	-------------------------------------	----------------	----------------	--------------	--------------	---------------	-------------------------------	-------------------------------	--------------

NOTE— Col. (1): Name of the object. Col. (2)–(3): Coordinates. Col. (4)–(5): Diameter of the major and minor axis of the nebula. Col. (6)–(7): Main and Sub morphological type. Col. (8): Planetary nebula class with “T” meaning “True”, “L” meaning “Likely”, and “P” meaning “Possible”. Col. (9): Grade of the source assigned in our visual recovery. Col. (10): Notes on the source from our visual recovery. Col. (11)–(12): Galactic longitude and latitude. Col. (13): Reference catalog of the source.

References— 1—Preite-Martinez (1988); 2—Acker et al. (1992); 3—(Kohoutek 2001); 4—(Kerber et al. 2003); 5—(Kronberger et al. 2006); 6—(Mampaso et al. 2006); 7—(Parker et al. 2006a); 8—(Miszalski et al. 2008); 9—(Wesson et al. 2008); 10—(Miranda et al. 2009); 11—(Urquhart et al. 2009); 12—(Viironen et al. 2009a); 13—(Viironen et al. 2009b); 14—(Jacoby et al. 2010); 15—(Sabin et al. 2011); 16—(Viironen et al. 2011); 17—(Acker et al. 2012); 18—(Kronberger et al. 2014); 19—(Sabin et al. 2014); 20—(Kronberger et al. 2016); 21—(Le Dù 2017); 22—(Núñez et al. 2017); 23—(Fragkou et al. 2018); 24—uncataloged objects discovered with the Digital Sky Hunter (DSH; see proceedings associated with e.g., Kronberger et al. 2006; Jacoby et al. 2010); 25—uncataloged objects discovered by the amateur community; 26—uncataloged objects discovered as candidates in IPHAS.

REFERENCES

- Abell, G. O. 1966, ApJ, 144, 259, doi: [10.1086/148602](https://doi.org/10.1086/148602)
- Acker, A., Boffin, H. M. J., Outters, N., et al. 2012, RMxAA, 48, 223, doi: [10.48550/arXiv.1206.2477](https://doi.org/10.48550/arXiv.1206.2477)
- Acker, A., & Le Dù, P. 2014, L’Astronomie, 128, 40
- Acker, A., Marcout, J., Ochsenbein, F., et al. 1992, The Strasbourg-ESO Catalogue of Galactic Planetary Nebulae. Parts I, II.
- Akras, S., Leal-Ferreira, M. L., Guzman-Ramirez, L., & Ramos-Larios, G. 2019, MNRAS, 483, 5077, doi: [10.1093/mnras/sty3359](https://doi.org/10.1093/mnras/sty3359)
- Astropy Collaboration, Robitaille, T. P., Tollerud, E. J., et al. 2013, A&A, 558, A33, doi: [10.1051/0004-6361/201322068](https://doi.org/10.1051/0004-6361/201322068)
- Astropy Collaboration, Price-Whelan, A. M., Sipőcz, B. M., et al. 2018, AJ, 156, 123, doi: [10.3847/1538-3881/aabc4f](https://doi.org/10.3847/1538-3881/aabc4f)
- Astropy Collaboration, Price-Whelan, A. M., Lim, P. L., et al. 2022, ApJ, 935, 167, doi: [10.3847/1538-4357/ac7c74](https://doi.org/10.3847/1538-4357/ac7c74)
- Badenes, C., Maoz, D., & Ciardullo, R. 2015, ApJL, 804, L25, doi: [10.1088/2041-8205/804/1/L25](https://doi.org/10.1088/2041-8205/804/1/L25)
- Balick, B., & Frank, A. 2002, ARA&A, 40, 439, doi: [10.1146/annurev.astro.40.060401.093849](https://doi.org/10.1146/annurev.astro.40.060401.093849)
- Barentsen, G., Farnhill, H. J., Drew, J. E., et al. 2014, MNRAS, 444, 3230, doi: [10.1093/mnras/stu1651](https://doi.org/10.1093/mnras/stu1651)
- Bojićić, I. S., Parker, Q. A., & Frew, D. J. 2017, in Planetary Nebulae: Multi-Wavelength Probes of Stellar and Galactic Evolution, ed. X. Liu, L. Stanghellini, & A. Karakas, Vol. 323, 327–328, doi: [10.1017/S1743921317003234](https://doi.org/10.1017/S1743921317003234)
- Boumis, P., Akras, S., Xilouris, E. M., et al. 2006, MNRAS, 367, 1551, doi: [10.1111/j.1365-2966.2006.10048.x](https://doi.org/10.1111/j.1365-2966.2006.10048.x)
- Bunker, A. J., Warren, S. J., Hewett, P. C., & Clements, D. L. 1995, MNRAS, 273, 513, doi: [10.1093/mnras/273.2.513](https://doi.org/10.1093/mnras/273.2.513)
- Chambers, K. C., Magnier, E. A., Metcalfe, N., et al. 2016, arXiv e-prints, arXiv:1612.05560, doi: [10.48550/arXiv.1612.05560](https://doi.org/10.48550/arXiv.1612.05560)
- Ciardullo, R., Feldmeier, J. J., Jacoby, G. H., et al. 2002, ApJ, 577, 31, doi: [10.1086/342180](https://doi.org/10.1086/342180)
- Ciardullo, R., Jacoby, G. H., Ford, H. C., & Neill, J. D. 1989, ApJ, 339, 53, doi: [10.1086/167275](https://doi.org/10.1086/167275)
- Cohen, M., Parker, Q. A., Green, A. J., et al. 2011, MNRAS, 413, 514, doi: [10.1111/j.1365-2966.2010.18157.x](https://doi.org/10.1111/j.1365-2966.2010.18157.x)
- Condon, J. J., Cotton, W. D., Greisen, E. W., et al. 1998, AJ, 115, 1693, doi: [10.1086/300337](https://doi.org/10.1086/300337)
- Condon, J. J., Kaplan, D. L., & Terzian, Y. 1999, ApJS, 123, 219, doi: [10.1086/313236](https://doi.org/10.1086/313236)
- Cook, D. O., Kasliwal, M. M., Van Sistine, A., et al. 2017, in American Astronomical Society Meeting Abstracts, Vol. 229, American Astronomical Society Meeting Abstracts #229, 237.08
- Cook, D. O., Kasliwal, M. M., Van Sistine, A., et al. 2019, ApJ, 880, 7, doi: [10.3847/1538-4357/ab2131](https://doi.org/10.3847/1538-4357/ab2131)
- Corradi, R. L. M., Mampaso, A., Viironen, K., et al. 2005, in American Institute of Physics Conference Series, Vol. 804, Planetary Nebulae as Astronomical Tools, ed. R. Szczerba, G. Stasińska, & S. K. Gorny, 7–10, doi: [10.1063/1.2146213](https://doi.org/10.1063/1.2146213)
- Corradi, R. L. M., Valentini, M., Munari, U., et al. 2010, A&A, 509, A41, doi: [10.1051/0004-6361/200913231](https://doi.org/10.1051/0004-6361/200913231)
- De Marco, O., & Moe, M. 2005, in American Institute of Physics Conference Series, Vol. 804, Planetary Nebulae as Astronomical Tools, ed. R. Szczerba, G. Stasińska, & S. K. Gorny (AIP), 169–172, doi: [10.1063/1.2146264](https://doi.org/10.1063/1.2146264)
- Dopita, M. A., Vassiliadis, E., Wood, P. R., et al. 1997, ApJ, 474, 188, doi: [10.1086/303444](https://doi.org/10.1086/303444)
- Drew, J. E., Greimel, R., Irwin, M. J., et al. 2005, MNRAS, 362, 753, doi: [10.1111/j.1365-2966.2005.09330.x](https://doi.org/10.1111/j.1365-2966.2005.09330.x)
- Eisenstein, D. J., Weinberg, D. H., Agol, E., et al. 2011, AJ, 142, 72, doi: [10.1088/0004-6256/142/3/72](https://doi.org/10.1088/0004-6256/142/3/72)
- Ford, H. C., & Jenner, D. C. 1978, in Bulletin of the American Astronomical Society, Vol. 10, 665
- Fragkou, V., Parker, Q. A., Bojićić, I. S., & Aksaker, N. 2018, MNRAS, 480, 2916, doi: [10.1093/mnras/sty1977](https://doi.org/10.1093/mnras/sty1977)
- Frank, A., Balick, B., & Riley, J. 1990, AJ, 100, 1903, doi: [10.1086/115646](https://doi.org/10.1086/115646)
- Frew, D. J. 2017, in Planetary Nebulae: Multi-Wavelength Probes of Stellar and Galactic Evolution, ed. X. Liu, L. Stanghellini, & A. Karakas, Vol. 323, 11–19, doi: [10.1017/S1743921317003507](https://doi.org/10.1017/S1743921317003507)
- Frew, D. J., & Parker, Q. A. 2005, in American Institute of Physics Conference Series, Vol. 804, Planetary Nebulae as Astronomical Tools, ed. R. Szczerba, G. Stasińska, & S. K. Gorny, 11–11, doi: [10.1063/1.2146214](https://doi.org/10.1063/1.2146214)
- Frew, D. J., & Parker, Q. A. 2010, PASA, 27, 129, doi: [10.1071/AS09040](https://doi.org/10.1071/AS09040)
- Froebrich, D., Makin, S. V., Davis, C. J., et al. 2015, MNRAS, 454, 2586, doi: [10.1093/mnras/stv1729](https://doi.org/10.1093/mnras/stv1729)
- Fujita, S. S., Ajiki, M., Shioya, Y., et al. 2003, ApJL, 586, L115, doi: [10.1086/374859](https://doi.org/10.1086/374859)
- Garrett, J. 2021, SciencePlots (v1.0.9), 1.0.9, Zenodo, Zenodo, doi: [10.5281/zenodo.4106649](https://doi.org/10.5281/zenodo.4106649)
- González-Solares, E. A., Walton, N. A., Greimel, R., et al. 2008, MNRAS, 388, 89, doi: [10.1111/j.1365-2966.2008.13399.x](https://doi.org/10.1111/j.1365-2966.2008.13399.x)

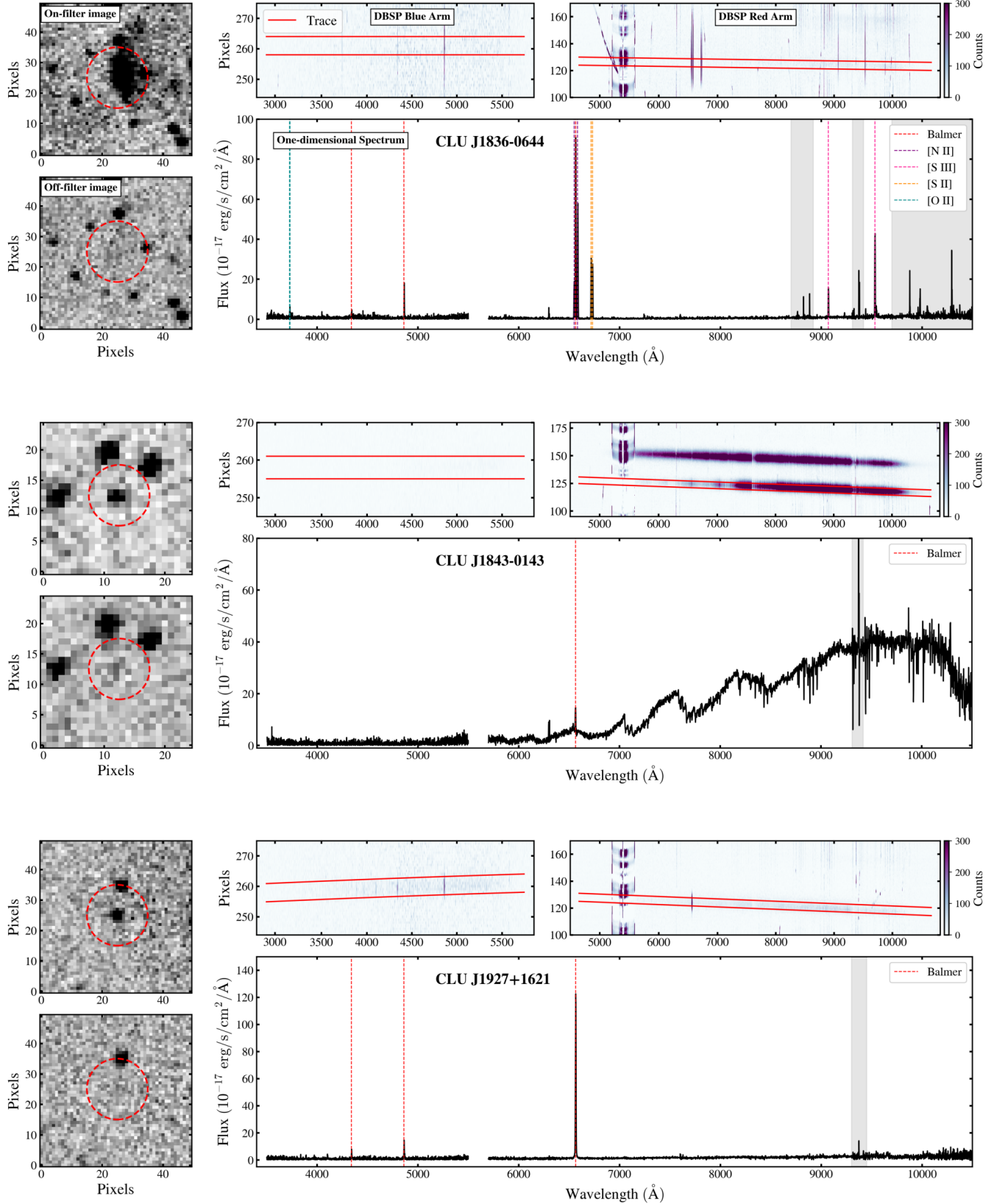


Figure B1. DBSP follow-up spectra for (from top to bottom) CLU J183648.44–064442.8, CLU J184324.79–014319.2, and CLU J192710.49+162128.6. In each figure, **Left panel:** shows the CLU images (top: ON/H α filter, bottom: OFF filter), **Two upper-right panels:** two-dimensional DBSP spectra for the blue and red channels respectively, with the trace marked, and **Lower-right panel:** the one-dimensional spectra extracted from the marked trace. The identified prominent are marked and the contaminated portions of the spectra are shaded. We have omitted the extreme ends of the blue and red arms ($\simeq 5400 - 5800 \text{ \AA}$) due to significantly elevated noise in this break region.

- Górny, S. K. 2006, in Planetary Nebulae in our Galaxy and Beyond, ed. M. J. Barlow & R. H. Méndez, Vol. 234, 409–410, doi: [10.1017/S1743921306003486](https://doi.org/10.1017/S1743921306003486)
- Haro, G. 1951, PASP, 63, 144, doi: [10.1086/126345](https://doi.org/10.1086/126345)
- Harris, C. R., Millman, K. J., van der Walt, S. J., et al. 2020, Nature, 585, 357, doi: [10.1038/s41586-020-2649-2](https://doi.org/10.1038/s41586-020-2649-2)
- Hunter, J. D. 2007, Computing in Science and Engineering, 9, 90, doi: [10.1109/MCSE.2007.55](https://doi.org/10.1109/MCSE.2007.55)
- Iben, I., J. 1995, PhR, 250, 2
- Irabor, T., Hoare, M. G., Oudmaijer, R. D., et al. 2018, MNRAS, 480, 2423, doi: [10.1093/mnras/sty1929](https://doi.org/10.1093/mnras/sty1929)
- Jacob, R., Schönberner, D., & Steffen, M. 2013, A&A, 558, A78, doi: [10.1051/0004-6361/201321532](https://doi.org/10.1051/0004-6361/201321532)
- Jacoby, G. H. 1989, ApJ, 339, 39, doi: [10.1086/167274](https://doi.org/10.1086/167274)
- Jacoby, G. H. 1997, in The Extragalactic Distance Scale, ed. M. Livio, M. Donahue, & N. Panagia, 197, doi: [10.48550/arXiv.astro-ph/9608128](https://doi.org/10.48550/arXiv.astro-ph/9608128)
- Jacoby, G. H., & Van de Steene, G. 2004, A&A, 419, 563, doi: [10.1051/0004-6361:20035809](https://doi.org/10.1051/0004-6361:20035809)
- Jacoby, G. H., Kronberger, M., Patchick, D., et al. 2010, PASA, 27, 156, doi: [10.1071/AS09025](https://doi.org/10.1071/AS09025)
- Jones, A. M., Gledhill, T. M., Froebrich, D., & Smith, M. D. 2018, MNRAS, 480, 1563, doi: [10.1093/mnras/sty1931](https://doi.org/10.1093/mnras/sty1931)
- Kennicutt, Robert C., J., Bresolin, F., French, H., & Martin, P. 2000, ApJ, 537, 589, doi: [10.1086/309075](https://doi.org/10.1086/309075)
- Kerber, F., Mignani, R. P., Guglielmetti, F., & Wicenec, A. 2003, A&A, 408, 1029, doi: [10.1051/0004-6361:20031046](https://doi.org/10.1051/0004-6361:20031046)
- Kohoutek, L. 2001, A&A, 378, 843, doi: [10.1051/0004-6361:20011162](https://doi.org/10.1051/0004-6361:20011162)
- Kron, R. G. 1980, ApJS, 43, 305, doi: [10.1086/190669](https://doi.org/10.1086/190669)
- Kronberger, M., Teutsch, P., Alessi, B., et al. 2006, A&A, 447, 921, doi: [10.1051/0004-6361:20054057](https://doi.org/10.1051/0004-6361:20054057)
- Kronberger, M., Jacoby, G. H., Ciardullo, R., et al. 2012, IAU Symposium, 283, 414, doi: [10.1017/S1743921312011696](https://doi.org/10.1017/S1743921312011696)
- Kronberger, M., Jacoby, G. H., Acker, A., et al. 2014, in Asymmetrical Planetary Nebulae VI Conference, ed. C. Morisset, G. Delgado-Inglada, & S. Torres-Peimbert, 48
- Kronberger, M., Parker, Q. A., Jacoby, G. H., et al. 2016, in Journal of Physics Conference Series, Vol. 728, Journal of Physics Conference Series, 072012, doi: [10.1088/1742-6596/728/7/072012](https://doi.org/10.1088/1742-6596/728/7/072012)
- Kuhn, M. A., de Souza, R. S., Krone-Martins, A., et al. 2021, ApJS, 254, 33, doi: [10.3847/1538-4365/abe465](https://doi.org/10.3847/1538-4365/abe465)
- Kwitter, K. B., & Henry, R. B. C. 2022, PASP, 134, 022001, doi: [10.1088/1538-3873/ac32b1](https://doi.org/10.1088/1538-3873/ac32b1)
- Kwok, S. 2005, Journal of Korean Astronomical Society, 38, 271, doi: [10.5303/JKAS.2005.38.2.271](https://doi.org/10.5303/JKAS.2005.38.2.271)
- Kwok, S., Purton, C. R., & Fitzgerald, P. M. 1978, ApJL, 219, L125, doi: [10.1086/182621](https://doi.org/10.1086/182621)
- Law, N. M., Kulkarni, S. R., Dekany, R. G., et al. 2009, PASP, 121, 1395, doi: [10.1086/648598](https://doi.org/10.1086/648598)
- Le Dû, P. 2017, L'Astronomie, 131, 46
- Le Dû, P., Mulato, L., Parker, Q. A., et al. 2022, A&A, 666, A152, doi: [10.1051/0004-6361/202243393](https://doi.org/10.1051/0004-6361/202243393)
- LeCun, Y., Bengio, Y., & Hinton, G. 2015, Nature, 521, 436, doi: [10.1038/nature14539](https://doi.org/10.1038/nature14539)
- Lee, J. C., Ly, C., Spitler, L., et al. 2012, PASP, 124, 782, doi: [10.1086/666528](https://doi.org/10.1086/666528)
- Lintott, C. J., Schawinski, K., Slosar, A., et al. 2008, MNRAS, 389, 1179, doi: [10.1111/j.1365-2966.2008.13689.x](https://doi.org/10.1111/j.1365-2966.2008.13689.x)
- Ly, C., Lee, J. C., Dale, D. A., et al. 2011, ApJ, 726, 109, doi: [10.1088/0004-637X/726/2/109](https://doi.org/10.1088/0004-637X/726/2/109)
- Maciel, W. J., & Costa, R. D. D. 2003, in Planetary Nebulae: Their Evolution and Role in the Universe, ed. S. Kwok, M. Dopita, & R. Sutherland, Vol. 209, 551
- Mampaso, A., Corradi, R. L. M., Viironen, K., et al. 2006, A&A, 458, 203, doi: [10.1051/0004-6361:20054778](https://doi.org/10.1051/0004-6361:20054778)
- Miranda, L. F., Pereira, C. B., & Guerrero, M. A. 2009, AJ, 137, 4140, doi: [10.1088/0004-6256/137/5/4140](https://doi.org/10.1088/0004-6256/137/5/4140)
- Miszalski, B., Acker, A., Parker, Q. A., & Moffat, A. F. J. 2009, A&A, 505, 249, doi: [10.1051/0004-6361/200912176](https://doi.org/10.1051/0004-6361/200912176)
- Miszalski, B., Parker, Q. A., Acker, A., et al. 2008, MNRAS, 384, 525, doi: [10.1111/j.1365-2966.2007.12727.x](https://doi.org/10.1111/j.1365-2966.2007.12727.x)
- Moe, M., & De Marco, O. 2006, ApJ, 650, 916, doi: [10.1086/506900](https://doi.org/10.1086/506900)
- Núñez, A., Agüeros, M. A., Covey, K. R., & López-Morales, M. 2017, ApJ, 834, 176, doi: [10.3847/1538-4357/834/2/176](https://doi.org/10.3847/1538-4357/834/2/176)
- Oke, J. B., & Gunn, J. E. 1982, PASP, 94, 586, doi: [10.1086/131027](https://doi.org/10.1086/131027)
- Osterbrock, D. E., & Ferland, G. J. 2006, Astrophysics of gaseous nebulae and active galactic nuclei
- Paczynski, B. 1971a, AcA, 21, 417
—. 1971b, Astrophys. Lett., 9, 33
- Parker, Q., Bojicic, I., Frew, D., et al. 2014, in Asymmetrical Planetary Nebulae VI Conference, ed. C. Morisset, G. Delgado-Inglada, & S. Torres-Peimbert, 69
- Parker, Q. A. 2022, Frontiers in Astronomy and Space Sciences, 9, 895287, doi: [10.3389/fspas.2022.895287](https://doi.org/10.3389/fspas.2022.895287)
- Parker, Q. A., Bojičić, I. S., & Frew, D. J. 2016, in Journal of Physics Conference Series, Vol. 728, Journal of Physics Conference Series, 032008, doi: [10.1088/1742-6596/728/3/032008](https://doi.org/10.1088/1742-6596/728/3/032008)
- Parker, Q. A., Phillipps, S., Pierce, M. J., et al. 2005, MNRAS, 362, 689, doi: [10.1111/j.1365-2966.2005.09350.x](https://doi.org/10.1111/j.1365-2966.2005.09350.x)

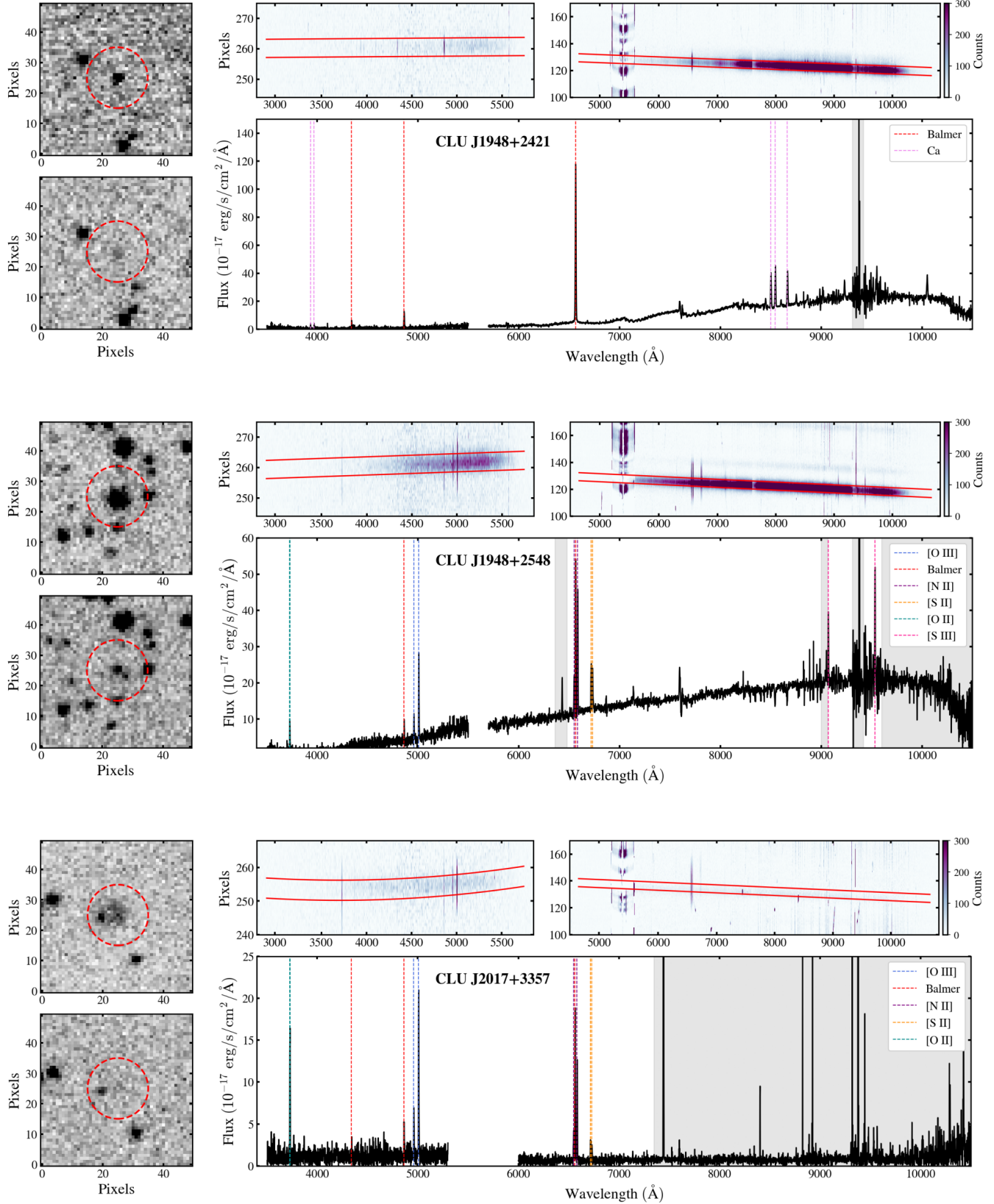


Figure B1 continued. DBSP follow-up spectra for (from top to bottom) CLU J194817.60+242116.7, CLU J194804.17+254848.6, and CLU J201756.61+335718.2. Same format as Figure B1.

- Parker, Q. A., Acker, A., Frew, D. J., et al. 2006a, MNRAS, 373, 79, doi: [10.1111/j.1365-2966.2006.10950.x](https://doi.org/10.1111/j.1365-2966.2006.10950.x)
- . 2006b, VizieR Online Data Catalog: MASH Catalogues of Planetary Nebulae (Parker+ 2006-2008), VizieR On-line Data Catalog: V/127A. Originally published in: 2006MNRAS.373...79P
- Parker, Q. A., Cohen, M., Stupar, M., et al. 2012, MNRAS, 427, 3016, doi: [10.1111/j.1365-2966.2012.21927.x](https://doi.org/10.1111/j.1365-2966.2012.21927.x)
- Pascual, S., Gallego, J., Aragón-Salamanca, A., & Zamorano, J. 2001, A&A, 379, 798, doi: [10.1051/0004-6361:20011389](https://doi.org/10.1051/0004-6361:20011389)
- Perek, L., & Kohoutek, L. 1967, Catalogue of Galactic Planetary Nebulae
- Preite-Martinez, A. 1988, A&AS, 76, 317
- Prochaska, J., Hennawi, J., Westfall, K., et al. 2020a, The Journal of Open Source Software, 5, 2308, doi: [10.21105/joss.02308](https://doi.org/10.21105/joss.02308)
- Prochaska, J., Hennawi, J., Cooke, R., et al. 2020b, pypeit/PypeIt: Release 1.0.0, v1.0.0, Zenodo, doi: [10.5281/zenodo.3743493](https://doi.org/10.5281/zenodo.3743493)
- Rau, A., Kulkarni, S. R., Law, N. M., et al. 2009, PASP, 121, 1334, doi: [10.1086/605911](https://doi.org/10.1086/605911)
- Roberson, M. S., Fremling, C., & Kasliwal, M. M. 2021, DBSP_DRP: DBSP Data Reduction Pipeline, Astrophysics Source Code Library, record ascl:2108.020, <http://ascl.net/2108.020>
- Sabin, L., Corradi, R. L. M., & Mampaso, A. 2011, in Revista Mexicana de Astronomia y Astrofisica Conference Series, Vol. 40, Revista Mexicana de Astronomia y Astrofisica Conference Series, 183–184
- Sabin, L., Zijlstra, A. A., Wareing, C., et al. 2010, PASA, 27, 166, doi: [10.1071/AS09046](https://doi.org/10.1071/AS09046)
- Sabin, L., Parker, Q. A., Corradi, R. L. M., et al. 2014, MNRAS, 443, 3388, doi: [10.1093/mnras/stu1404](https://doi.org/10.1093/mnras/stu1404)
- Sánchez Contreras, C., Sahai, R., Gil de Paz, A., & Goodrich, R. 2008, ApJS, 179, 166, doi: [10.1086/591273](https://doi.org/10.1086/591273)
- Scheuermann, F., Kreckel, K., Anand, G. S., et al. 2022, MNRAS, 511, 6087, doi: [10.1093/mnras/stac110](https://doi.org/10.1093/mnras/stac110)
- Skrutskie, M. F., Cutri, R. M., Stiening, R., et al. 2006, AJ, 131, 1163, doi: [10.1086/498708](https://doi.org/10.1086/498708)
- Sobral, D., Best, P. N., Matsuda, Y., et al. 2012, MNRAS, 420, 1926, doi: [10.1111/j.1365-2966.2011.19977.x](https://doi.org/10.1111/j.1365-2966.2011.19977.x)
- Sobral, D., Best, P. N., Geach, J. E., et al. 2009, MNRAS, 398, 75, doi: [10.1111/j.1365-2966.2009.15129.x](https://doi.org/10.1111/j.1365-2966.2009.15129.x)
- Stroe, A., & Sobral, D. 2015, MNRAS, 453, 242, doi: [10.1093/mnras/stv1555](https://doi.org/10.1093/mnras/stv1555)
- Sun, R., Li, Y., Parker, Q., et al. 2024, MNRAS, 528, 4733, doi: [10.1093/mnras/stad3954](https://doi.org/10.1093/mnras/stad3954)
- Taylor, M. B. 2005, in Astronomical Society of the Pacific Conference Series, Vol. 347, Astronomical Data Analysis Software and Systems XIV, ed. P. Shopbell, M. Britton, & R. Ebert, 29
- Urquhart, J. S., Hoare, M. G., Purcell, C. R., et al. 2009, A&A, 501, 539, doi: [10.1051/0004-6361/200912108](https://doi.org/10.1051/0004-6361/200912108)
- van der Walt, S., Colbert, S. C., & Varoquaux, G. 2011, Computing in Science and Engineering, 13, 22, doi: [10.1109/MCSE.2011.37](https://doi.org/10.1109/MCSE.2011.37)
- van Dokkum, P. G. 2001, PASP, 113, 1420, doi: [10.1086/323894](https://doi.org/10.1086/323894)
- Viironen, K., Mampaso, A., Corradi, R. L. M., et al. 2009a, A&A, 502, 113, doi: [10.1051/0004-6361/200811575](https://doi.org/10.1051/0004-6361/200811575)
- Viironen, K., Greimel, R., Corradi, R. L. M., et al. 2009b, A&A, 504, 291, doi: [10.1051/0004-6361/200912002](https://doi.org/10.1051/0004-6361/200912002)
- Viironen, K., Mampaso, A., Corradi, R. L. M., et al. 2011, A&A, 530, A107, doi: [10.1051/0004-6361/201014897](https://doi.org/10.1051/0004-6361/201014897)
- Wenger, M., Ochsenbein, F., Egret, D., et al. 2000, A&AS, 143, 9, doi: [10.1051/aas:2000332](https://doi.org/10.1051/aas:2000332)
- Wesson, R., Barlow, M. J., Corradi, R. L. M., et al. 2008, ApJL, 688, L21, doi: [10.1086/594366](https://doi.org/10.1086/594366)
- Wright, E. L., Eisenhardt, P. R. M., Mainzer, A. K., et al. 2010, AJ, 140, 1868, doi: [10.1088/0004-6256/140/6/1868](https://doi.org/10.1088/0004-6256/140/6/1868)